SINGLE CELL ANALYSIS ON MICROFLUIDIC DEVICES

by

YANLI CHEN

B.S., Shanghai University, 2000
M.S., East China Normal University, 2003

A THESIS

submitted in partial fulfillment of the requirements for the degree

MASTER OF SCIENCE

Department of Chemistry
College of Arts And Sciences

KANSAS STATE UNIVERSITY
Manhattan, Kansas

2008

Approved by:

Major Professor
Christopher Culbertson

Copyright

Abstract

A microfluidic device integrated with valves and a peristaltic pump was fabricated using multilayer soft lithography to analyze single cells. Fluid flow was generated and mammalian cells were transported through the channel manifold using the peristaltic pump. A laser beam was focused at the cross-section of the channels so fluorescence of individual labeled intact cells could be detected. Triggered by the fluorescence signals of intact cells, valves could be actuated so fluid flow was stopped and a single cell was trapped at the intersection. The cell was then rapidly lysed through the application of large electric fields and injected into a separation channel. Various conditions such as channel geometry, pumping frequency, control channel size, and pump location were optimized for cell transport. A Labview program was developed to control the actuation of the trapping valves and a control device was fabricated for operation of the peristaltic pump. Cells were labeled with a cytosolic dye, Calcein AM or Oregon Green, and cell transport and lysis were visualized using epi-fluorescent microscope. The cells were transported at rates of ~ 1mm/s. This rate was optimized to obtain both high throughput and single cell trapping. An electric field of 850-900 V/cm was applied so cells could be efficiently lysed and cell lysate could be electrophoretically separated. Calcein AM and Oregon Green released from single cells were separated and detected by laser-induced fluorescence. The fluorescence signals were collected by PMT and sampled with a multi-function I/O card. This analyzing method using microchip may be applied to explore other cellular contents from single cells in the future.

Table of Contents

List of Figures

List of Tables

Acknowledgements

I would like to thank my research advisor, Prof. Christopher Culbertson for all the help and consideration during my graduate study.

I also want to thank my graduate committee members, Prof. Paul Smith and Prof. Takashi Ito for their efforts to my graduation.

I enjoyed working with all current and previous members in Prof. Culbertson's group. Amanda Meyer, Kurt Hoeman, Scott Klasner, Alex Price, Pernilla Viberg, , Manuja Lamabadusuriya, Kevin McDaniels have given me useful discussions advices about my research. I am so grateful to work with our previous group member, Dr. Greg Roman, who has solved numerous problems for me.

Also I would like to thank Dr. Anne Culbertson who has spent a lot time teaching me skills of cell culture and providing cells for me.

I am particularly grateful to Ms. Earline Dikeman for providing care and numerous help during my life here.

And finally, I would like to give my greatest gratitude to my husband, Zhiqang Yang, and my parents. They have given me solid support and great love all the time.

Chapter 1-Introduction

Single cell analysis has developed rapidly in recent years due to its importance in better understanding cell biology or physiology. The investigation of how biological systems respond to the dynamics of environmental stimuli can help to determine the causes of many diseases. Microfluidic technologies provide a progressive platform to analyze single cells.

1.1 Introduction to cells and single cell analysis

1.1.1 General information of cells

Cells are complex biochemical entities and contain a number of different kinds of molecules. In addition to major organelles such as the mitochondria, nucleus and lysozomes etc, there exist numerous various molecular components including proteins, DNA, RNA, phospholipids, carbohydrates and small molecules including ions and transient radical species[1]. Cell membranes consist of phospholipids and proteins which function to control the exchange of molecules between cells and extracellular environment. Organelle membranes have a composition similar to the cell membrane and isolate the organelles from the remaining cellular environment. The complexities of cellular analysis arise from the wide ranges in concentrations and in types of compounds present in cells. Different phases in cell cycle contribute to the difference in cell behavior and cellular contents. The concentration of different proteins can vary by several orders of magnitude. The type of proteins can change due to oxidation, phosphorylation, or glycosylation. A eukaryotic cell normally has size of 5-20μm and thus has volume of only 0.1-8pL[2]. Due to the tiny size of the cells, the contents such as DNA, mRNA and proteins within the cells are present in low copy number. In a normal cell only 1-2 copies of a specific DNA sequence are present, so the concentration of a gene is on the order of 10^{-12} M. Also, some cellular proteins such as signaling enzymes have an absolute number of 1,000-10,000[3]. So it is necessary to have techniques that can handle and detect low numbers of molecules in such small volumes.

Figure1.1 General depiction of the eukaryotic cell[1].

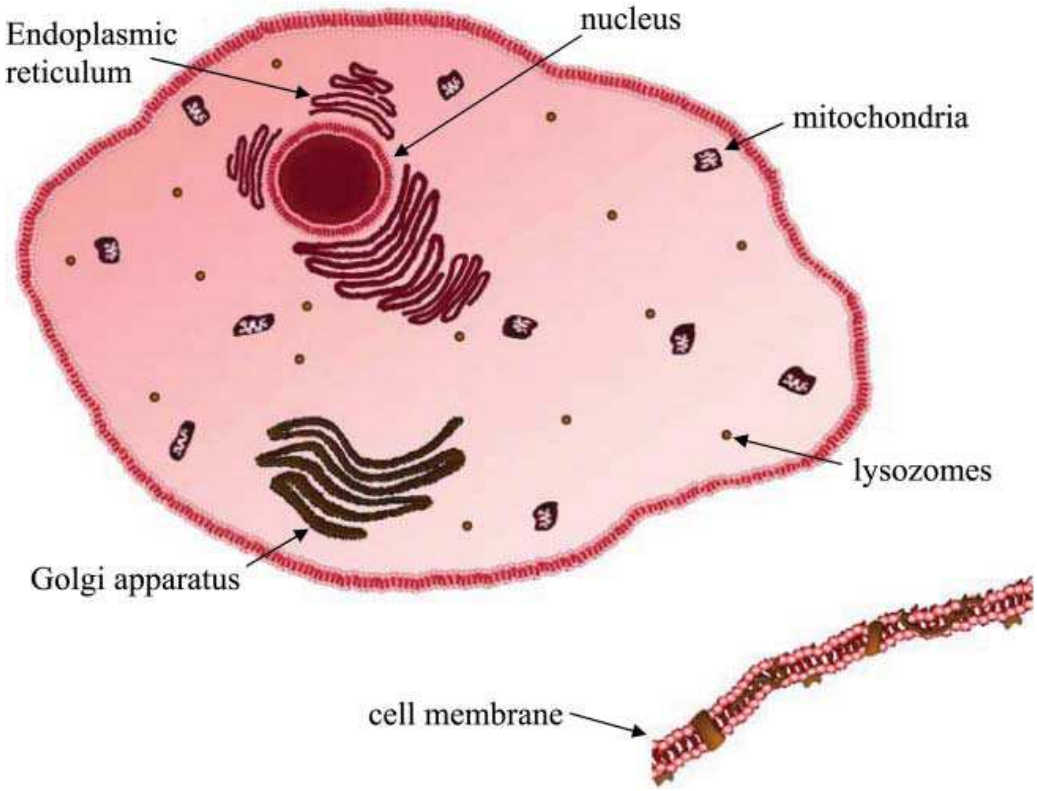

1.1.2 Analysis of kinase activity

Kinases are enzymes that can modify other proteins by phosphorylation. Kinases can affect many cellular behaviors including cell growth and differentiation, cell shape and locomotion, and metabolism. Up to 30% of proteins may be modified by kinase activity and kinases play a significant role in regulating signaling pathways. By switching on or off in a pathway, kinases can either activate or repress signaling events. Most kinases act on serine/threonine and function at the beginning of signaling transduction cascades, while some kinases act on tyrosine and function throughout cascades[4]. Kinase activity can be regulated by phosphorylation and binding with activator proteins or inhibitor proteins. Mutations of kinases may result in many diseases, especially cancer.

Consequently, investigating kinase activity is important to understand signaling pathways and determine the cause of diseases.

1.1.3 Single cell analysis

In conventional analytical methods, many cells are analyzed simultaneously so information from individual cells is lost. Individual cells are heterogeneous in chemical composition and biological activity. Single cells can produce thousands of different proteins, lipids, hormones and metabolites. Single cells behave distinctively in response to the same stimuli in timing and concentration even though they are the same type of cells[4] partly due to probabilistic behaviors in the signaling pathways. Especially when cancer cells progress, the physiology of in individual cells diverges more and more widely. Bulk techniques may allow one to obtain average information and intracellular interactions but they do not provide actual distribution of intracellular contents. Because of the heterogeneity within a population, it's essential to use an appropriate technique to investigate them individually in order to better understand their biochemical behavior in the intricate signaling network and distinguish abnormal cells from a large amount of healthy cells to diagnose specific diseases. Meanwhile, single cell analysis has developed rapidly in cell manipulation, cell culture, cell lysis and intracellular component detection. Capillary electrophoresis is a high efficiency separation technique and is suitable for the analysis of single cells when coupled with high sensitivity detection such as LIF. Recently many types of single cell analysis have been successfully performed using Capillary Electrophoresis[5,6,7]. Allbritton's group has reported fast electrical lysis and separation of chemical analytes within single cells by CE coupled with LIF[8]. The cell was lysed by electrical field generated between a gold-coated electrode on the capillary tip and a second electrode beneath the cell prior to rapid sampling of cellular lysate into the capillary. This was followed by electrophoretic injection and separation of cytosolic dyes such as Oregon Green and 6-carboxyfluorescein. In addition, they also reported separation of kinase peptide substrates in their phosphorylated and native forms[9, 10]. Although CE is efficient, it can't avoid the problem of long separation times and low throughput. Alternatively, microfluidic devices provide a way to achieve rapid, high throughput analysis. McClain et al. have reported a microfluidic device that can rapidly lyse the cells by electrical fields and separate the molecules within the cytosol in less than

2.2 s^{11}. These analysis rates were 100-1000 times faster than that can be obtained by traditional CE.

1.2 Microfluidic devices

Microfluidic devices are composed of fluid filled channels and chambers with critical dimensions of tens to hundreds of micrometers. Microfluidic devices have shown several advantages over many other analytical techniques for single cell analysis. First, microfluidic devices have a small scale and low cost of production. Eukaryotic cells normally have a volume of 0.1-8pL; so the ability of microfluidic devices to handle volumes as small as 1pL makes them suitable to handle such single cells. Since small volume of samples and reagents are needed during the analysis, both cost and waste can be greatly reduced, and the cells can be analyzed more rapidly. Due to the small size of channels, analytes released from cells, even those at very low concentrations can be detected because of little dilution after lysis. Otherwise, if using traditional methods which can only deal with analytes in large volumes, those originally low concentration analytes such as specific proteins or enzymes will be diluted by a thousand to a million times which dilutes it below the concentration detection limit. Second, microfluidic devices can control cell movement and reagents mixing and perfusion more precisely by either valve control or electrokinetic control. Fluidic flow in microfluidic channels is mostly laminar because the Reynolds number for fluid flow in microfluidic devices is generally <0.1. Laminar flow helps fluidic streamlines in microchannels remain constant over time and multiple microfluidic streamlines that merge will flow smoothly next to each other without any turbulent mixing. The only mixing occurs by the diffusion across the interface of streams. Since diffusion is only rapid for small molecules in microscale devices, cells will not flow out of their input stream. This characteristic of laminar flow in microfluidic device provides the potential to pattern cells and their environment. Thus, Laminar flow in microfluidic devices can be used to produce different spatial concentrations in a highly discrete manner. By utilizing laminar flow composed of two merging streams, cells can be exposed to soluble hormone epidermal growth factor selectively and mitochondria in each half of a single cell could be labeled with a different fluorescent dye[3]. Third, these devices can achieve faster separations than CE by applying higher electrical fields because the large surface to volume ratio of the channels and the

high thermal conductivity of the substrate materials can transport heat away rapidly. Thus microfluidic devices can achieve rapid separation which can be in a matter of seconds for electrophoresis-based separations and provide a high throughput analytical platform which is essential to single cell analysis since large numbers of single cells need to be examined in order to detect cells with abnormal behaviors. Lu's group was able to analyze Calcein released from cells at rates up to 75-85 cells/min[12]. Fourth, microfluidic devices raise the possibility for portability associated with automation and disposability due to its small size and low cost material. Fifth, microfluidic devices have the capacity to integrate multiple functions such as cell transport and manipulation, cell culture, cell sorting, cell lysis, and intracellular analytes separation on one chip. Sixth, parallel analysis can be achieved on microfluidic devices so a large number of targets can be analyzed simultaneously. Quake's group has developed a microfluidic device that can perform 72 parallel 450-pL reverse transcriptase-PCR's which enables high throughput single cell gene expression analysis[13]. Kennedy's group has reported a microfluidic chip containing four individual channel networks that can monitor cellular secretion from multiple independent living samples[14]. Finally, sensitive detection can be more efficiently coupled on microfluidic devices due to its flat optical interfaces.

Figure 1.2 RT-PCR device. Left, photograph of the device loaded with food dye. Right, Optical micrographs of eight reaction chambers and one reaction chamber[13].

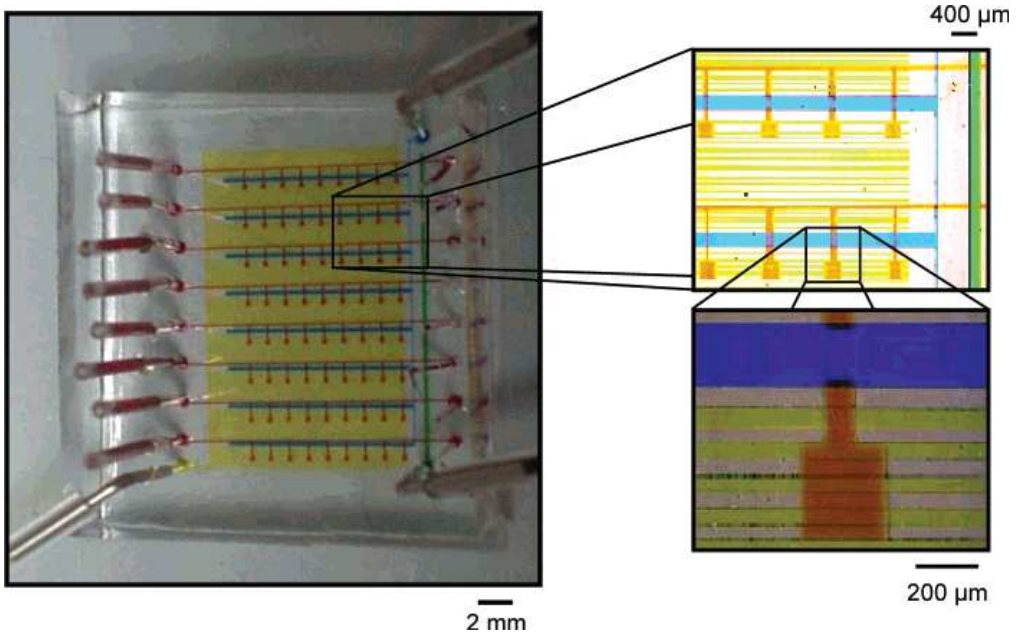

Figure 1.3 (A), Pattern of laminar flow[15]. (B), Solution of epidermal growth factor (EGF) is presented in red color and a cell was stimulated by EGF by diffusion[3].

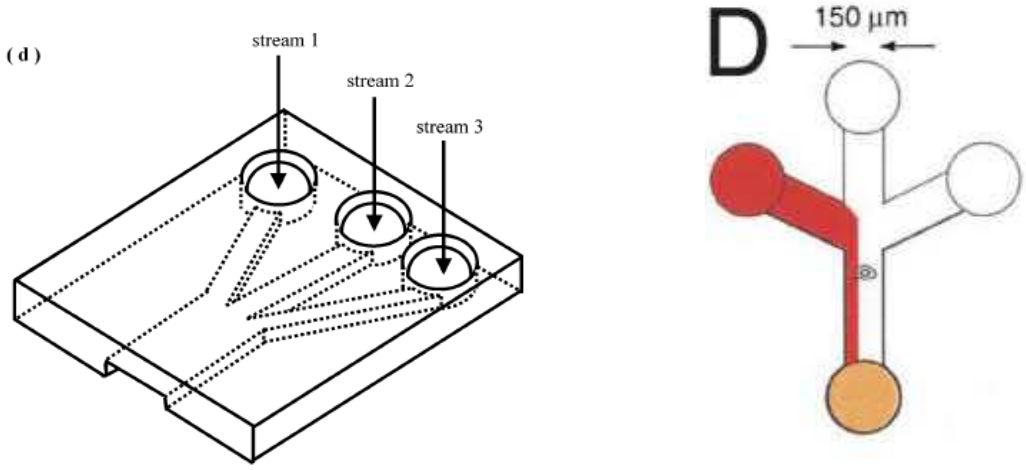

(A) **(B)**

1.3 Single cell analysis on microfluidic devices

1.3.1 Organelle isolation

In order to separate the proteins or other biomolecules residing in the cytoplasm or inside the subcellular component, it is necessary to isolate or segregate the organelles so that they don't interfere with the analysis. Organelle isolation is traditionally performed on bench in bulk cells, i.e. sedimentation, which can only provide average information of organelles and make it impossible to carry out real time monitoring at the molecular level. Even within the same cell, organelles may be heterogonous in enzymatic activity or response to pharmaceutical treatment. The measurement of individual organelle properties can manifest the diversity in organelle function, thus reveal organelle malfunction in diseased cells. Arriaga's group has reported the electrophoretic separation of individual mitochondria[16], nuclei[17] and liposome[3, 18] by CE with LIF detection. Also they demonstrated drug (doxorubicin) distribution in both mitochondria and nuclei by measuring organelle drug content using CE-LIF and MEKC-LIF respectively[19, 20]. Microfluidic devices improve organelle analysis in many aspects including raising the selectivity for the organelles of interest even with the presence of other organelles and reducing the chance of damaging and altering biological functions[21]. In addition, it facilitates single cell organelle analysis integrated with other functions such as investigation of molecules released from organelles.

1.3.2 Methods of cell lysis on microfluidic devices

Both organelle characterization and cellular content detection require cells to be lysed to obtain individual organelles or biomolecules such as proteins DNAs, or mRNAs from cells. The method of cell lysis is critical in studying biological molecules within single cells because it determines what kind of intracellular processes can be measured. Conventionally cells can be lysed by mechanical or chemical means. Mechanical lysis doesn't need reagents and is usually performed by forces such as centrifugation that can break down organelle membranes. Kim and coworkers have demonstrated a method to mechanically lyse the cell on a microfluidic compact disc by the inter-particle force generated by the friction and collision between cells and beads[22]. There also demonstrations of lysing cells mechanically by forcing cells through nanostructured

barbs. After cell lysis, quantitative measurements of accessible protein were acquired[23]. Chemical lysis is mostly performed to extract protein from cells by using ionic surfactants to solubilize lipid membranes as well as subcellular membranes. And it can also be integrated with cellular composition analysis on chip by delivering lysing reagent before separation. Although using nonionic surfactants to lyse the cell can selectively disrupt the outer cell membrane and keep the organelles intact[17], it takes more than 250 seconds to complete lysis. It is only suitable to investigate DNA, RNA or proteins, whose concentrations change slowly with time. Yager's group has demonstrated a microfluidic device with lysis channel and detection channel in parallel[24]. This device performed cell lysis by mixing with a lysing detergent. A large intracellular enzyme, β-galactosidase was extracted and detected after derivitization of the protein on chip. Many biological reactions occur on time scales of seconds or less. During the signal transduction pathway such as phosphorylation of proteins by kinases, the concentration of the proteins can change by more than an order of magnitude in less than 1 s. Therefore there is a high probability that another signal transduction pathway can be triggered or the concentration of analytes is altered in the time that it takes the chemical lysis to occur. For rapid processes, reactions need to be terminated at a high temporal resolution. In order to get accurate measurement of the analytes, it is necessary to have a way to lyse the cell in milliseconds or faster so as to completely terminate these rapid reactions. Electrical lysis shows advantages of rapidly lysing the cells and selectively breaking down cells outer membrane without disrupting the organelle membrane. Ramsey's group has achieved complete cell lysis within 33ms on a microchip integrated with cell manipulation[11], cell lysis and efficient separation of fluorescent cytosol dyes.

Figure 1.4 (A) Scanning electron micrograph of a mechanical cell lysis device with nanoscale barbs[23]. (B) Cell transport, cell lysis and lysate injection and electrophoretic separation in microchannels[11]. (C) Schematic of microfluidic channels for cell lysis and fractionation/detection of intracellular components[24]. (D) Phase-contrast microscopy of cells that were electroporated[25].

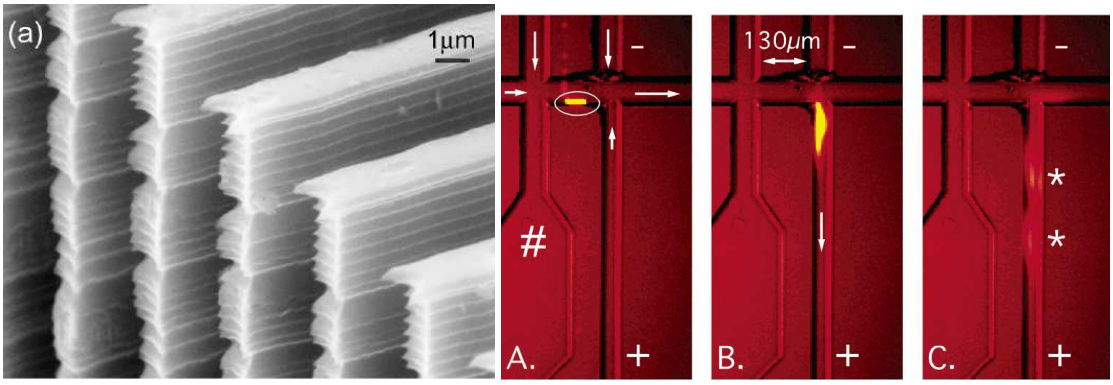

(A) **(B)**

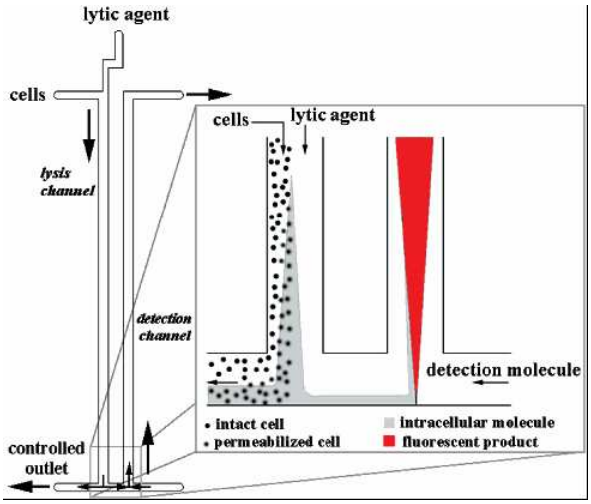

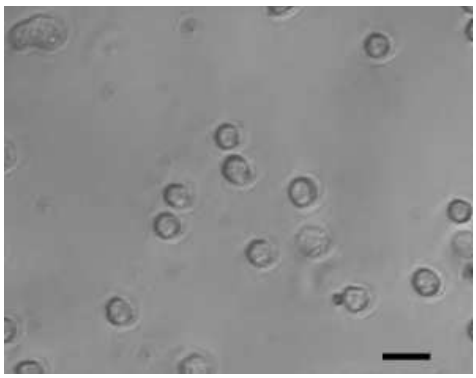

(C) **(D)**

The bilayer lipid membrane of cells serves as a barrier to hydrophilic molecules and ions. When an electric field applied across the plasma membrane exceeds the dielectric strength of a cell membrane, the membrane conductance increases dramatically. In addition, the applied electrical field causes reorientation of those charged or polar molecules in the membrane and results in the formation of pores so that large hydrophilic molecules can enter the cells. The localized Joule heating on the membrane also contributes to the membrane breakdown.[26] This has been an effective way to introduce

DNA, protein or drugs into the cells. Cells can recover after removal of the electric field when the potential is under 1V of transmembrane potential. Above that value, the irreversible breakdown of cell membrane can take place. When an electrical field is between 300-1000V/cm with duration in microseconds to milliseconds, cells can be completely lysed[27]. It is possible to breakdown the cell membrane but not the organelle membrane because the ratio of the radius of the extracellular membrane to electrical field is significantly different from that of plasma membrane. With the existence of an external electric field, the cells can be modeled using an equivalent RC circuit. Equation (1.1) and (1.2)[25] shows the transmembrane potential for the cells and organelles, where E is the external field strength, R the radii of particles, C the capacitance of the membranes per unit area, r resistivity, ω the frequency of the applied electric field, and E_{int} the intracellular field strength. The subscript org denotes organelle, α for the extracellular electrolyte, i for intracellular electrolyte (cytoplasm), and s for intra-organelle electrolyte.

$$V_{mem} = \frac{1.5ER}{(1 + I\omega RC(r_i + r_a / 2))} \quad \text{.....(equation 1.1)}$$

$$V_{org} = \frac{1.5E_{\text{int}} R_{org}}{1 + I\omega R_{org} C_{org} (r_s + r_i / 2)} \quad \text{..... (equation 1.2)}$$

$$E_{\text{int}} = \frac{1.5E}{1 + (1/[I\omega RC(r_i + [r_a / 2])])} \quad \text{..... (equation 1.3[25])}$$

Figure 1.5[25] demonstrates how frequency relates to the transmembrane potential. As we can see, there is a frequency range where transmembrane potential for the plasma membrane is significantly different from the organelle membrane, thus the plasma membrane can be broken down without affecting the organelle membrane.

Figure 1.5 transmembrane potential trend toward change of frequency for cells and organelles[25].

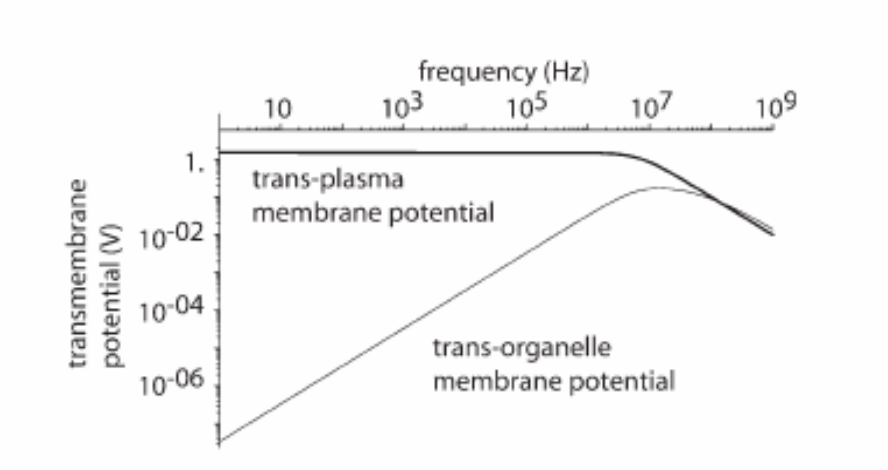

Figure 1.6 Polarization and induction of the transmembrane potential in the cell membrane by positioning a cell in an electric field of strength E[28].

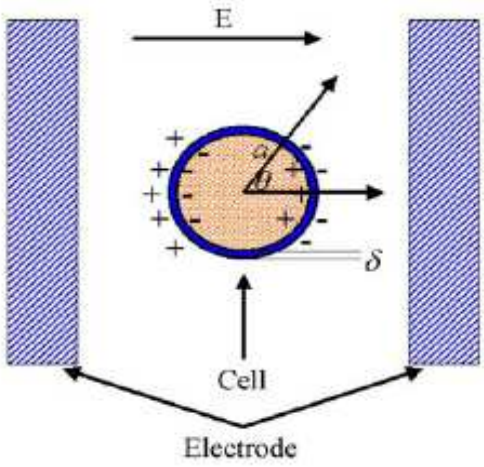

The efficiency of cell lysis is affected by frequencies, applied voltage and medium osmolarity. Cell lysis is initiated by the electric field and the lysis rate has a linear relationship with the applied voltage[28] as shown in figure 1.8[26]. Due to the relationship between electric field and the width of the channel as shown in equation 1.5[30]:

$$\frac{E_2}{E_1} = \frac{W_1}{W_2}$$ (equation 1.4),

When the voltage is applied across the entire channel, the narrow section (Figure 1.7) of the channel can result in much higher field strength than the wide section. Both Lee and Lim's group has proved that cell lysis rate decreases as frequency increases or as shorter pulse width is applied[28, 31]. Cell lysis takes place more rapidly in the hypotonic or hypertonic buffers than in the isotonic buffer, which indicates that the hypo/hyperosmolarity of the medium contributes to the formation of electropores[30].

Figure 1.7 The schematic of the microfluidic electroporation[26].

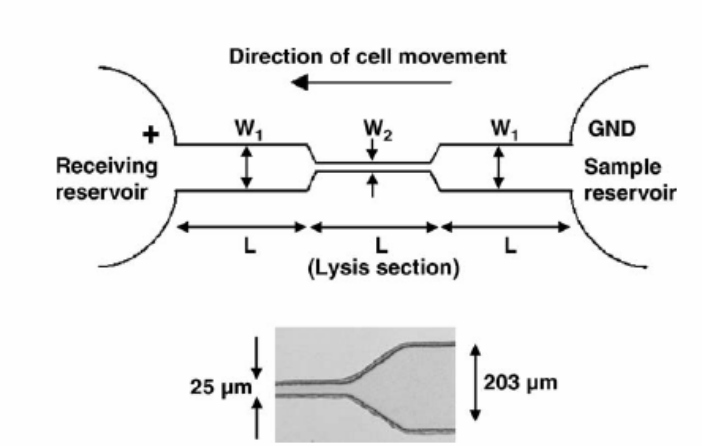

Figure 1.8 Left: Lysis rate vs. applied voltage. Right: Lysis rate vs. frequency[28].

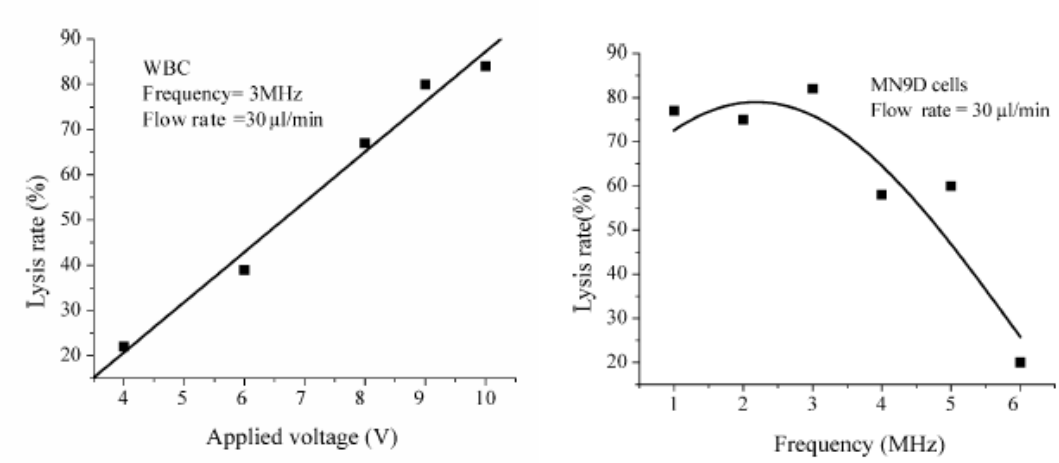

1.3.3 Cell transport and isolation on microfluidic devices

Transporting cells to precise locations without perturbing the analyte of interest in the cell on microchips is also an important issue during any cell analysis process including cell lysis. There are several methods to accurately position the cells. Electrokinetic and electro-osmotic driven-flow are implemented to transport cells in the channels but reports show that it may increase cell stress and activate signal transduction. Recently, optical tweezers are used to precisely move and locate cells to a desired destination, but the throughput is quite low. Among all the methods, hydrodynamic flow is most commonly used and is usually achieved by pneumatic pumping via the application of an external pressure applied at one of the microchip reservoirs. Hydrodynamic flow is gentile and can transport cells without causing cell damage, but it has the drawbacks that it is difficult to change the cell velocity and it is impossible to stop or dock the cell accurately during its movement. A pumping method called peristaltic pumping which integrates valves on chip can facilitate consistent and accurate flow control without external equipment. Cell confinement can improve lysate injection efficiency during the process of cell lysis. Cell trapping can be achieved by stopping fluidic flow from both sides using PDMS valves integrated on the chip. Integrated pumps and valves can be fabricated by a method termed multilayer soft lithography which was first demonstrated by Quake's group using polydimethylsiloxane (PDMS) as substrate material[32]. PDMS is largely used in the fabrication of microfluidic devices because it is inexpensive and easy to prototype. In addition, due to its high biocompatibility, optical transparency and high O_2 diffusion rates, PDMS microchips have been applied to many biochemical operations including cell culture[33], cell sorting[34], and biochemical separation[35]. For example, Jayaraman's group has reported a microfluidic device containing upstream dilution module and downstream cell culture chambers[36]. Diverse soluble stimuli were generated in upstream fluidic network and used to stimulate downstream reporter cells to monitoring dynamic gene expression.

In the microvalve and pumping system, valves are located at the intersection of a working fluidic channel and an air-filled actuation channel in two separate layers. Since the membrane between working and actuation channels is thin enough, it can deflect downward to close the working channel and block the fluid when pressure is applied

through the control channel. Three valves arranged on one working channel can form a peristaltic pump.

Figure 1.9 Schematic of peristaltic pump[32].

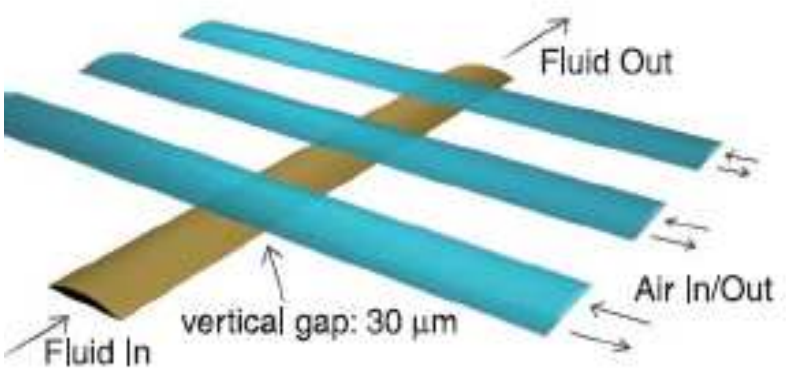

By adjusting the parameters such as delay phase between sequential valves, actuation pressure and frequency value, fluid can be pumped at a flow rate up to 7.5μL/min[37]. Integrating PDMS valves and pumps on microchips allows one to isolate cells by actuating two valves after a single cell is detected arriving between these two valves. Quake's group and some others have reported many applications of valves and pumps integrated on microchip. Martin's group has used injection valves to make injections of continuous-flow sample from a microfluidic channel to a capillary to carry out CE separation[38]. Integrated valves and pumps can also make accurate delivery of reagent which helps implement multiple functions on one chip. As Quake's group has reported, reagents such as lysis buffer, elution buffer or wash buffer would be delivered into the cell chamber respectively as desired by actuating the pump and valves, and all processes such as cell isolation, cell lysis, DNA and mRNA purification and recovery were performed on one chip[39]. The other advantage of using integrated valves and pump on chip is that it allows large scale integration and parallel assays on chip. Quake's group has demonstrated a high-density microfluidic memory storage device that contains thousands of valves and hundreds of chambers and deals with complex fluidic manipulation[40]. Also, they reported a microfluidic device that can perform sensitive 72 parallel RT-PCRs in 450-pL and detect β-actin transcripts from a total RNA template[41].

A variety of cell isolation methods have been developed during the process of cell analysis to address different aspects of environmental control, fast timescale measurements, image processing and isolation of secreted biomolecules. It is essential to isolate individual cells in a confined area since the concentration of macromolecules present in the cells is usually very low and cell isolation can prevent further dilution of originally low copy number substances eluted from cells. Cells can be captured by using physical barriers fabricated by PDMS[42]. Recently, droplet-based generation technologies have been reported to confine single cells. Aqueous droplets were dispensed into a non-aqueous stream and cells were trapped within the droplets. Then laminar streams of reagents were mixed with the droplet and allowed the reaction to occur for the captured cells. Once the captured single cell was photolysed by laser, the activity of intracellular enzyme was assayed by measuring the fluorescence intensity after combining with fluorescent substrates[43]. This paper also demonstrated cell trapping at the intersection by precise control of hydrodynamic flows or by systems of channels and structures, so reagents perfusion and pressure gradients can be well controlled. Microchambers can be used to isolate cells and concentrate secreted biomolecules. Microchambers can be generated by actuating integrated valves which terminate the fluidic flow inside microchannels. By conducting this method, gene expression of low copy number of β-galactosidase of single cells was monitored[44]. To trap and assay multiple cells simultaneously, one-dimensional or two-dimensional arrays are often used to provide high throughput analysis. Large quantities of individual cells can be analyzed simultaneously and image processing is simplified for well-ordered arrays. Tamiya's group has demonstrated a single-cell microassay chip with 30,000 microchambers, each of which accommodated single cells[45]. This method is suitable for high throughput single cell analysis of intracellular Ca^{2+} response and is applicable to screen antigen-specific lymphocytes for making monoclonal antibody. Thorsen's group developed a microfluidic array platform containing 576 chambers to screen cell cytotoxicity of mammalian cells[46]. Cell seeding and toxin exposure were carried out at a high throughput manner.

Figure 1.10 SEM images of microarray chip device[45].

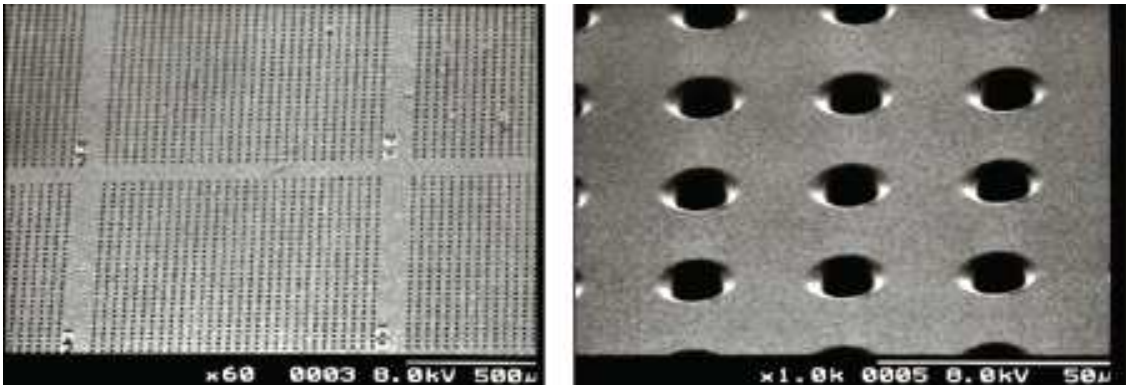

Figure 1.11 Composite image of microfluidic cytotoxicity array chip after toxin challenge and live/dead staining[46].

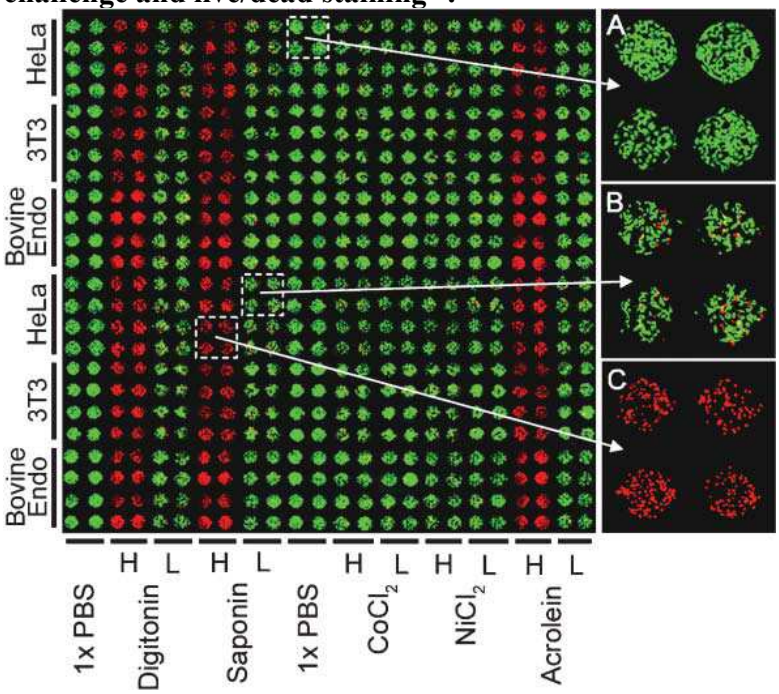

Figure 1.12 Left, Sequential images of the encapsulation of a single lymphocyte within an aqueous droplet surrounded by oil. Right, images of cell lysis by laser and fluorescent product of secreted enzyme and its substrate[3].

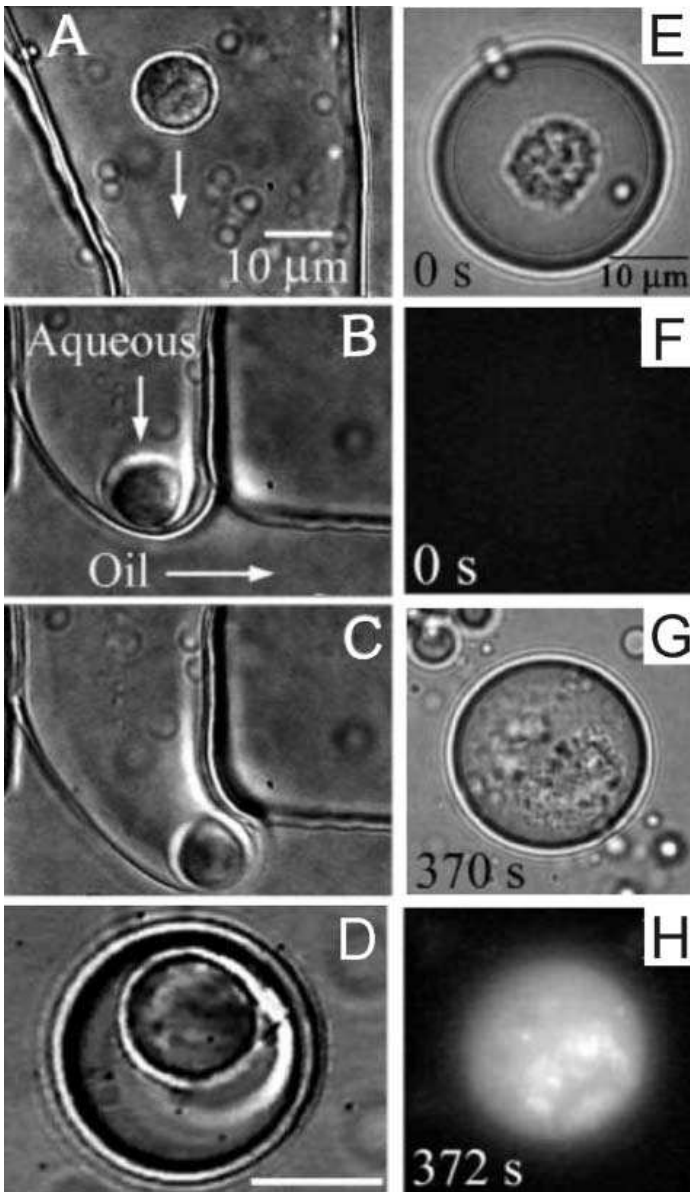

1.3.4 Imaging and Detection systems

Microscopy is a dominant tool for molecular imaging which can be used to detect presence and activity of cells as well as cellular substances. Fluorescent optical microscopes are used to image bio-molecules which have been derivatized by fluorescent

probes. Scanning thermal lens microscopy (TLM) was developed to analyze label-free single cells and secreted cytochrome-C from mitochondria was measured in real time as a single cell was exposed to an apoptosis-inducing agent[47]. Measurements of cellular analytes are usually performed by optical detection including Laser induced fluorescence (LIF) or chemiluminescence, electrochemical or mass spectrometric detection. Low concentrations of cellular constituents require a sensitive detection method. LIF is the most commonly used detection method because of its high sensitivity and low detection limits, which are essential to analyze single cells. Also, because many biomolecules have native fluorescence or can be derivatized to form fluorescent molecules, LIF becomes a convenient way to detect them. LIF systems use laser light to excite the fluorescent analyte and then collect the light emitted by analytes using a PMT. So cells or cellular contents usually need to be labeled with fluorescent dyes before the separation. LIF can be coupled with capillary electrophoresis or microfluidic devices to detect low concentrations of analytes after many handling processes. For example, Kennedy's group has reported a microfluidic device to perform on-line derivatization and detection of amino acid neurotransmitters by CE-LIF after push-pull perfusion sampling from the brain of live rats[48]. In recent years, light-emitting diodes (LED) have been used as an excitation source for fluorescence measurement, so the detection system can be miniaturized and can be disposable. An optical fiber was encapsulated inside the microchip and was used to direct light into microchannel for fluorescence detection[49]. The detection limit for LED excited detection system was about 25nmol L^{-1}. Electrochemical detection (EC) has the advantages of easy operation, low cost, selectivity and high sensitivity. EC converts chemical signals to voltage in microelectrodes and can be applied to detections of DNA fragments, amino acids, carbohydrates, and organic acids. Cho and co-workers have developed a microfluidic device that was used to measure the electrical impendence of red blood cells thus to distinguish normal and abnormal cells since there was significant difference of electrical impendence in magnitude and phase shift between normal and abnormal cells as shown in Figure 1.14[32]. In order to know the structural information of analytes, mass spectrometry (MS) can be coupled to separations by chip CE. MS has recently attracted more attention because of its ability to detect large biomolecules such as proteins with high sensitivity. One type of

detection method that attracts much interest is electro-spray ionization (ESI) MS which has a high sensitivity as shown in figure 1.13. Meanwhile, time of flight MS and matrix-assisted laser desorption ionization (MALDI) are also promising online coupling methods for single cell analysis[49].

Figure 1.13 Configuration of microspray and microchip[49].

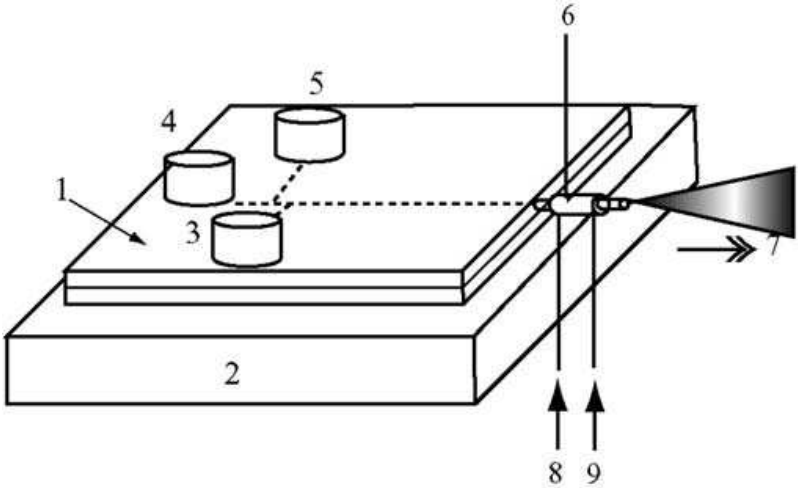

Figure 1.14 Electrical resistance measurement on twin microcantilever electrode[32].

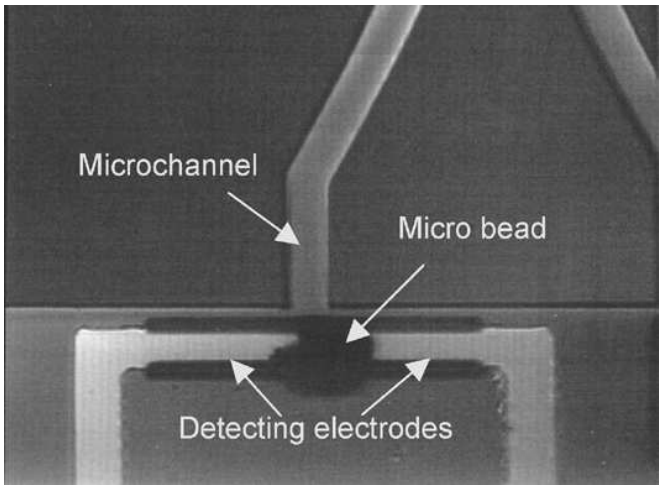

Figure 1.15 Electrical impedance of five kinds of media[32].

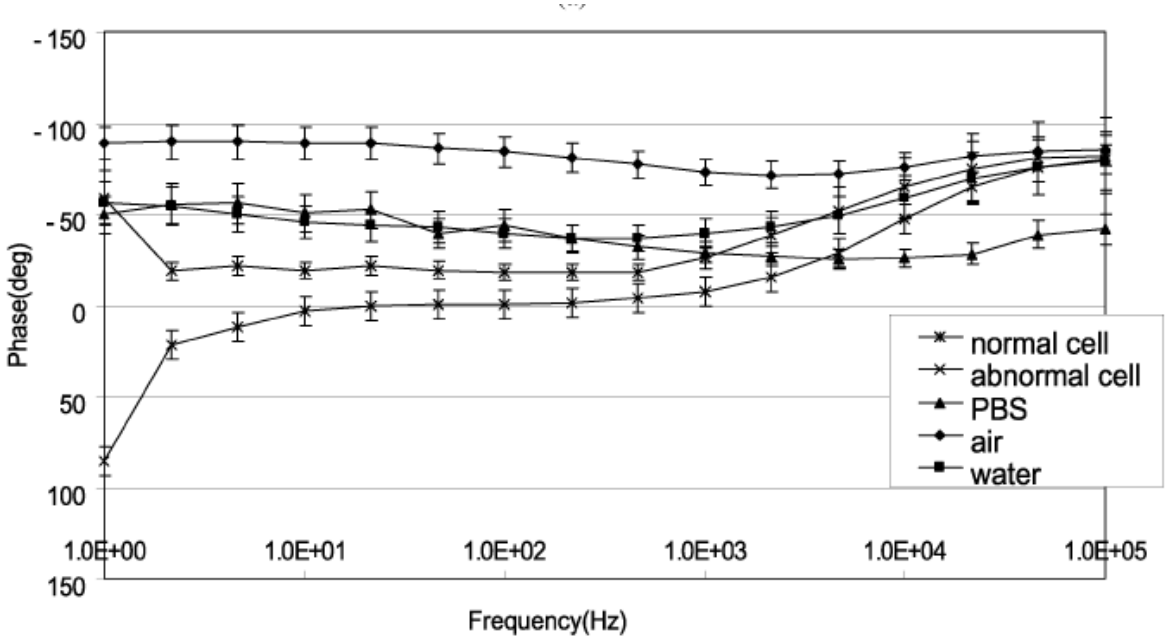

1.3.5 Analytical techniques for single cells

1.3.5.1 Separation of cell lysates by electrophoresis

There are several analytical techniques for quantification of cell lysates. Electrophoresis is widely used to separate analytes with different charge to mass ratio on microfluidic devices. In electrophoresis, the difference of charges on analytes results in their differential migration in external electric fields and leads to separations of these analytes. Increases in separation length and/or electrical field strength can result in enhancement of separation efficiency. During the separation of analytes electrokinetically on microchips, both electroosmotic and electrophoretic flows contribute to the transport of analytes but only the latter leads to a separation. One of the important advantages of using microfluidic devices is that the flow in the channel is laminar. In addition, the flow profile is flat across the cross-section of the channel. In microchannels, the surface of the channel is partially ionized. The resulting double layer containing excess charge causes the movement of ions in the bulk solution when an electric field is applied and the velocity of ions in the channel maintains constant which results in a planar flow profile.

In electrophoretic separations, ions move differently in an electric field and analytes are resolved by their electrophoretic mobilities. The electrophoretic mobility,

μ_{ep}, for an ion in an electric field takes place when friction or hydrodynamic force counterbalance the electric force.

$$\mu_{ep} = \frac{|z_i|e}{6\pi\eta r_i} \quad \text{.....(equation 1.6)}^{50}$$

where z is the magnitude of the charge for an ion I, e is the electronic charge, η is the viscosity of the fluid, and r_i is the radius of the ion. Electrophoretic velocity, u_{ep}, equal to the electrophoretic mobility times the electric field strength, E.

$u_{ep}=\mu_{ep}E$.....(equation 1.7)[50]

Separation efficiency can be expressed by Plate height (H) or plate number (N).

$$N = \frac{L^2}{\sigma^2} \quad \text{.....(equation 1.8)}^{50}$$

L is separation length and σ^2 is variance of concentration distribution of the band. The variance of analyte band width is the sum of different and independent variances including diffusion, Joule heating, the channel geometry, mass transfer effects and electrodispersion. In our experiment the separation distance, the magnitude of electric field, the channel geometry were optimized to minimize band broadening and obtain an efficient separation.

There are many reported applications of electrophoresis to separate amino acids, peptides, proteins or organelles. For example, Ramsey's group has reported a microchip with a long and spiral channel that separated 19 amino acids within 165 second[51]. To detect and analyze bio-molecules quantitatively, electrophoretic separation can be integrated on microfluidic systems. After separation, samples that exhibit fluorescence can be detected by passing by an optical detector. Ramsey's group also demonstrated a microchip that can perform cellular dyes separation integrated with cell manipulation and cell lysis and the total separation time was within 2.2 s[11]. And Kennedy's group used an electrophoresis-based immunoassay to monitor insulin secretion from single islets with a variety of glucose concentrations on a microfluidic device[52].

1***.3.5.2 Other analytical methods for single cells***

One quantitative method for protein analysis and detection is antibody capture. Antibody-based technology utilizes antigen-antibody binding achieve specificity in analysis. Channels can be coated with either solid supports or capture antibody and

analytes and secondary detection antibodies will be introduced into the channel subsequently[53]. Label-free detection methods including detection of changes in mass and electrical properties due to the binding on antibody functionalized sensor surface have become promising alternatives to fluorescence detection. Field-effective sensors with carbon nanotubes and silicon nanowires as the active sensing elements as well as mass-based sensors with cantilever technologies have shown high sensitivity and are able to detect femtomoles of proteins[53].

Figure 1.16 Left, electropherogram of Oregon green diacetate and its metabolites released from a single cell[11]. Right top, schematic of immunoassay performed using microbeads as solid support in a microfluidic system. Right bottom, schematic of a hollow cantilever –based mass sensor for analyte detection[53].

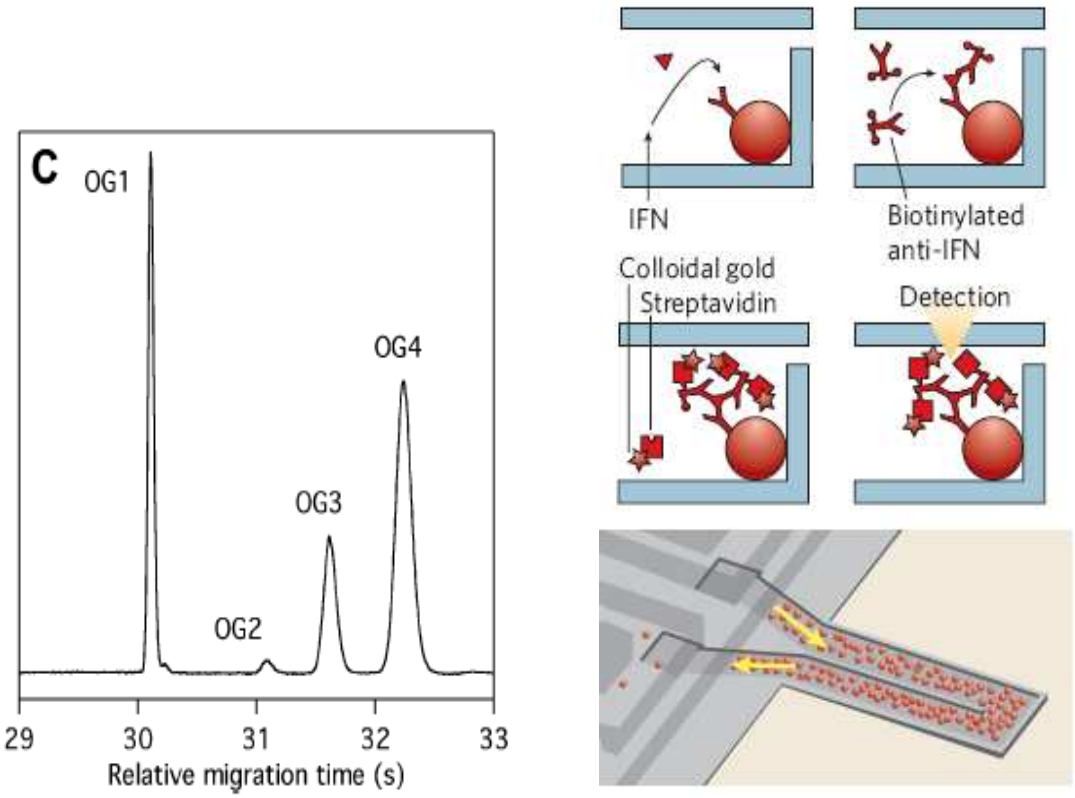

1.4 Applications

There are a variety of applications that can take advantage of capabilities of single cell based microfluidic devices. Cell manipulation such as cell culture[54, 55], cell sorting[56,

[57] and cell lysis[58, 59] have been performed on microfluidic devices. Recently, a microfluidic device that can separate and selectively concentrate live and dead bacteria cells by insulator-based dielectrophoresis (iDEP) has been reported[60]. Also, cellular content measurement[61, 62], gene expression[63-65], RT-PCR[33, 66, 67] and drug delivery[68, 69] have been implemented on microfluidic devices. For example, Harrison and co-workers have reported β-Galactosidase activity assay of single cell lysate on a microchip[70]. Jayaraman el. have demonstrated a microfluidic platform for dynamic expression of the activation of transcription factor NF-κB by delivering various concentration of cytokine TNF-α from upstream to downstream cultured cells[36]. Quake's group has developed a microfluidic device which can perform high parallel gene expression analysis. The device with integrated pneumatic valves was capable of cell lysis by introducing chemical lysis buffer, isolation of picogram and subpicogram messenger RNA templates and cDNA synthesis[66]. Lee's group fabricated a microfluidic device composed of U-shaped hydrodynamic trapping structure that allowed culture of single adherent cells in arrays and dynamic control of fluid perfusion with uniform environments for single cells[71]. Spence's group has been able to monitor intracellular nitric oxide (NO) production using fluorescence microscopy on a microfluidic device. The NO production was stimulated with adenosine triphosphate (ATP) using concentrations as low as 1μM which are similar to in vivo levels of ATP in the microcirculation[35].

Figure 1.17 AutoCAD drawing of a device with inputs and outputs labeled according to function. Rounded flow channels are depicted in green and control channels are shown in blue. Unrounded (rectangular profile) flow channels for affinity column construction are shown in red[66].

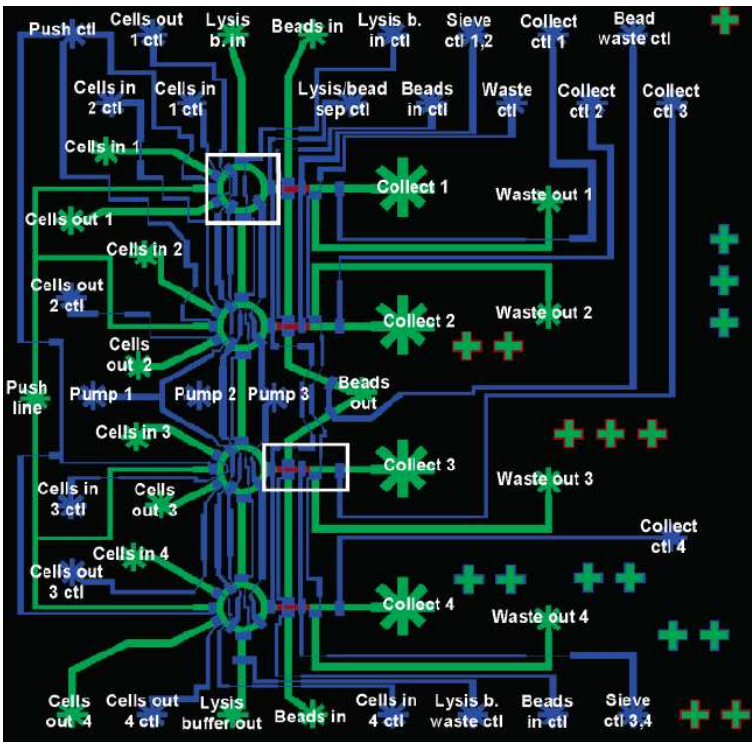

Figure 1.18 Single cell trapping arrays[71].

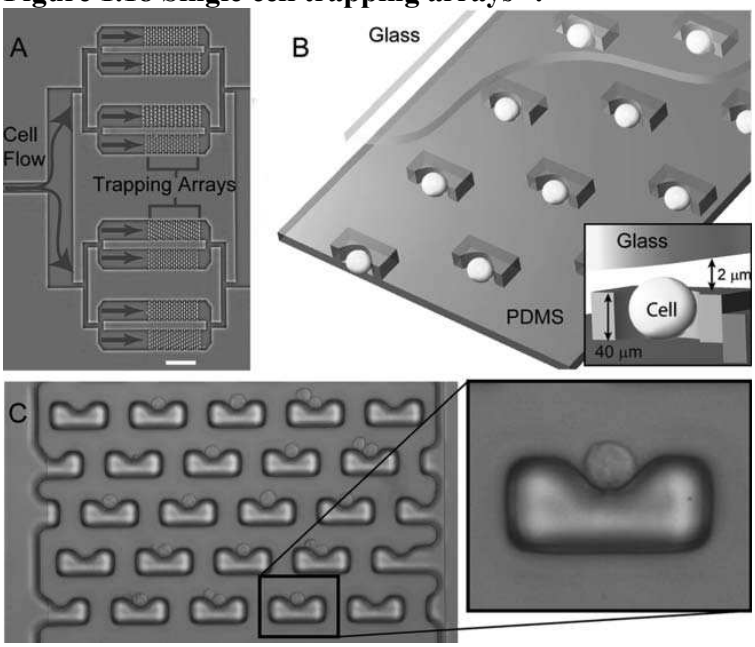

Chapter 2-Cell transport and isolation on microfluidic devices

2.1 Chip design

The monolithic chip was made from the silicone elastomer poly (dimethylsiloxane) (PDMS) and composed of two layers of channels. One was the thin fluidic channel layer where cell manipulation took place and the other thick layer was called control layer where the actuation of valves and pumps was executed. The thick layer was located above the thin working layer to have "push-down" geometry. This chip was designed for manipulation and analysis of mammalian cells which usually have the size of 10μm in dimension, so the channels were etched to 20μm deep to make enough space for single cell movement but meanwhile preventing channel clogging by cells when large numbers of cells flowed through the channel. The channels were 300μm wide and tapered to 80μm near the cross section except that the separation channel which was only 46μm wide. The narrower separation channel could reduce counter flow while a vacuum pressure was applied at the cell flow channel, thus enhancing cell lysate injection.

Figure 2.1 Schematic of the microchip[11]. Cells go through from cell reservoir to waste reservoir. Separation buffer runs from buffer reservoir in separation channel.

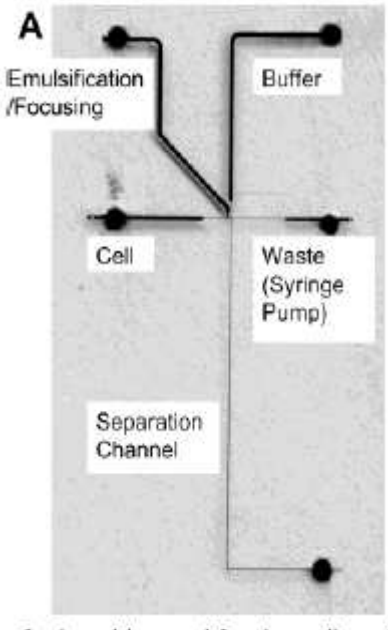

The control channels were designed to cross above where the fluid channels need to be closed. The on-off valve channels were 250μm wide and set above those tapered 80μm channels. This generated a 250×80μm active area. The valves for the peristaltic pump were set 125μm apart to avoid any interference with each other. All the control channels were 20μm deep.

Figure 2.2 Microscopic picture of the intersection of the microchip. Two layers of channels are shown. Blue channels stand for fluidic channels in the bottom layer; red channels stand for trapping valves in top layer; yellow channels represent for peristaltic pump in top layer.

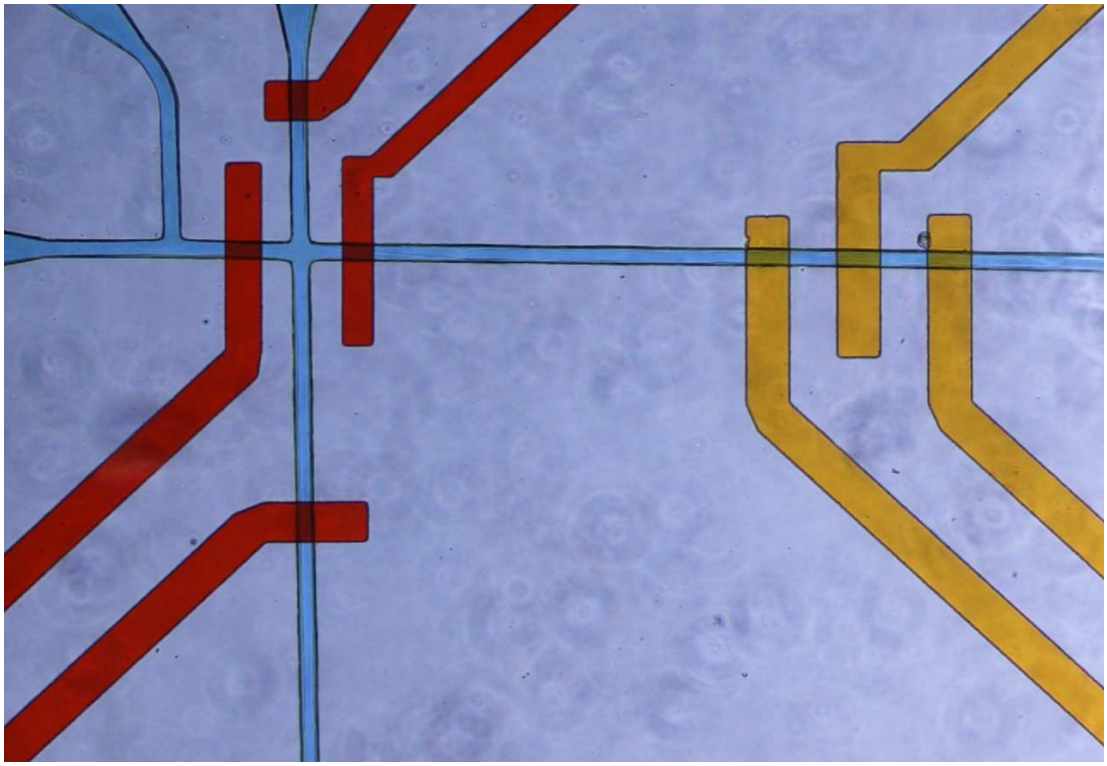

2.2 Fabrication of microchip with integrated valves and a peristaltic pump

2.2.1. Why we choose to use integrated valves and pumps on chips?

In previous research work it was hard to achieve complete lysate injection if individual cells were not confined in a certain area near the intersection. For this work,

cells were transported in glass chip channels by hydrodynamic flow. Single cells and their lysates were injected into the separation channel by applying a voltage to the channels perpendicular to the cell transport channel. It was difficult to achieve complete injection of the lysate because of the continuous flow through the transport channel since the pump was constantly on. The continuous cell flow resulted in partial cell lysate injection so not all the cell lysates could be detected. Integrated valves on chips provide a convenient way to control the flow. If the valves can block the fluidic flow when a cell reaches the intersection and the cell is confined in that area, a complete sample injection is more likely to happen and a better separation of cell lysate becomes potential. In addition, integrated pumping system can largely reduce dead volume and improve flow control.

2.2.2. How to fabricate chips by multilayer soft lithography?

The Polydimethylsiloxane (PDMS) has been shown to be an appropriate material for the fabrication of microfluidic channels using soft lithography. Soft lithography has the advantages of easy fabrication, rapid prototyping and cheapness. By curing the elastomer on a microfabricated mold, channels can be fabricated. To make integrated valves and pumps on a chip, a method termed multilayer soft lithography that combines soft lithography with bonding of multiple patterned elastomers is introduced[32].

By having each layer excess of one of the two curing components of the elastomer, the interface between the bottom and upper layers contains active molecules which can still react to generate irreversible bonding after curing these two layers together. Thus, the multilayer soft lithography makes it possible to fabricate 3-dimentional structures.

2.2.3. How valves work?

Valves are actuated simply by pushing Nitrogen gas into the valve channels. The membrane of elastomer between the channels is engineered to be as thin as 30-40μm, so when the pressure is applied to the control channel, the membrane deflects downward and closes the fluidic channel. Because the elastomer has the low Young's modulus, it is easy to deflect with small actuation force[32].

Figure 2.3 Schematic of valve actuation.

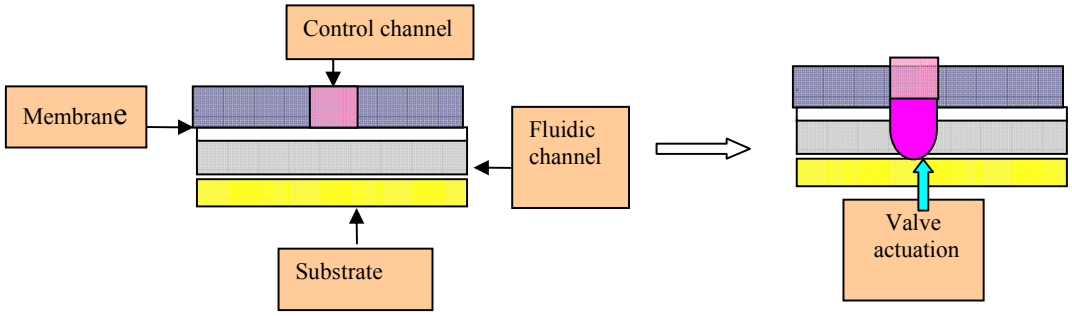

Making fluidic channels round is crucial in actuation of valves since at normal actuation pressure, only channels with a round cross section can be closed completely. The round shape transfers force from above to channel edge and close the channel from edge to center completely. However, channels with rectangular shape can only be closed partially under the same condition (See Figure 4). Channels can be made round by remolding the mold at high temperature.

Figure 2.4 Schematic of valve closing for square and round channel.

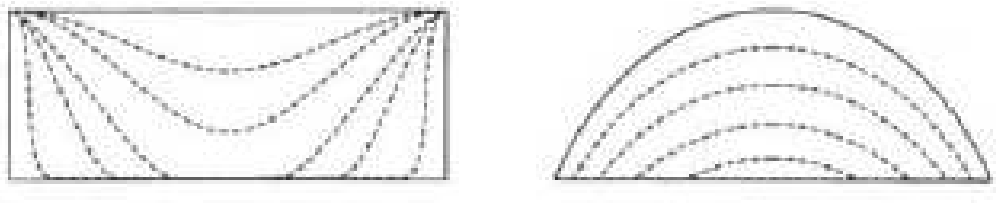

2.2.4 Fabricate flow channel master

The mold for flow channels was made out of positive photoresist AZ P4620. The glass slide was treated with vapor deposition of hexamethyldisilazane (HMDS) first to improve stickiness of photoresist to the glass substrate. The photoresist was spin coated at 450 rpm for 40s to produce a 20μm thick layer. The channels were obtained after the photoresist was baked at 110^{o}C for 3 min, pattered with transparency film by UV exposure at 50mW/cm^{2} for 9.3 sec and developed in AZ 400K developer for several

hours. To make the channels round, the channels were remolded by hard baking at 110^{o}C for 3 min. The depth and shape of the channels were measured using the profiler.

2.2.5 Fabrication of valve master mold

The valve channel master will be made out of SU-8 2035. This negative photoresist was spun at 2000 rpm for 30 sec. After being prebaking at 65^{o}C for 3 min and 95^{o}C for 5 min, the SU-8 was exposed under UV light at 50mW/cm^{2} for 9 sec. through a negative film. Then, the SU-8 was post baked at 60^{o}C for 1 min and 80^{o}C for 5 min before being developed. The valve had a manifold mold thickness of about 50μm.

2.2.6 Fabrication of PDMS chip

The working channel master was treated with HMDS to ensure complete release of PDMS layer from mold. Then the master was spin-coated with 20:1 mix of silicone elastomer and curing agent at 2000 rpm for 2 min to produce a 30μm thin membrane. The control channel master was also treated with HMDS and was cast with a 5:1 mix of same component as thick as 5mm to ensure mechanical stability. Both layers were baked in the 80^{o}C for 10 min. This period of time is appropriate for partially curing the PDMS but it will keep the surface active. Holes were punched with a 20-guage needle in the control layer, through which nitrogen was allowed to enter the control channels. The actuation layer was then peeled off and aligned with fluidic channel layer under the microscope. These two layers were cured together at 80^{o}C for 45 min to form monolithic layer. The cured PDMS layers were then peeled up from fluid layer master and holes served as reservoirs in the fluidic channels were created using a hole puncher. Finally, the PDMS layers were sealed onto a blank PDMS layer.

2.3 Actuation of valves and the peristaltic pump

2.3.1 How to actuate valves pneumatically?

To pneumatically actuate the valves on the chip, gas needs to be delivered to the control channels. In our experiment, Nitrogen was delivered from a tank through Teflon tubing to a valve manifold where eight 3-way facemount solenoid valves from the Lee Company had been assembled. Each solenoid valve was connected to a power supply control box that could control the opening or closing of the valves through a ribbon wire.

The power supply were wired to the NI-DAQ card, and a Labview program was used to control the on-off switch of the power supply to apply or remove a potential from the valves. With the power switched on, Nitrogen gas was transported into the microvalves in the chip, forcing the membrane to deflect and terminate the flow in the fluidic channel. With the power switch off, Nitrogen gas left the microvalve, leading to the relaxation of chamber and allowing the fluidic flow to resume in the fluidic channel. The fluidic channel was filled will fluorescent dyes to allow clear visualization of the opening and closing of the valves. Some results can be seen in the figure. If the actuation pressure exceeds the minimum requirement, it is possible for valves to be closed completely. The larger the active area the lower the pressure was needed. Also, the larger the pressure, the more likely the channel was completely closed. But higher pressure can cause gas leaking problems. Results showed that the pressure needed to fully close the valve was about 15-20 psi. Control channels were also filled with solution with 2% BSA in order to prevent gas leaking into the fluidic channels.

Figure 2.5 Microscope fluorescent picture of valve actuation. Fluid is blocked by actuation of control channel and no fluorescence can be visualized.

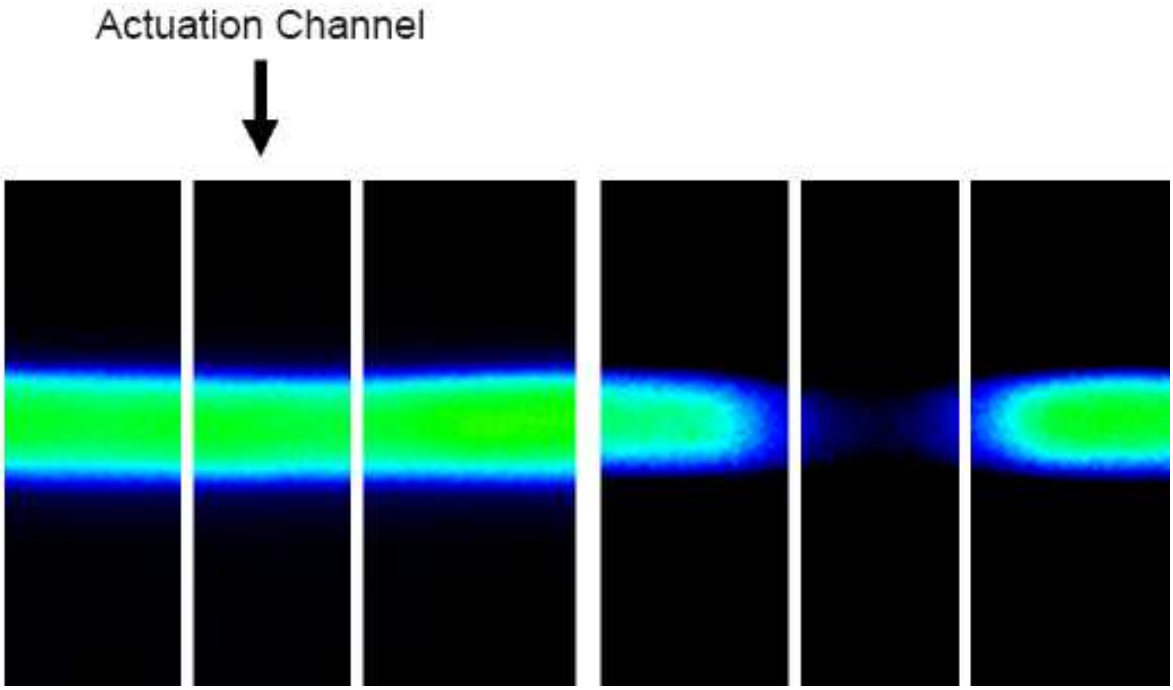

2.3.2 How to generate peristaltic pumping?

The peristaltic pump was composed of 3 sequentially actuated valves that were overlaid across one single fluidic channel. In collaboration with Electronic Design Lab (EDL), we designed and fabricated a control device for operating the peristaltic pump. With this device we could alter the cycle frequency and the delay phase. The control box was connected between solenoid valves and the power supply control unit. When the box was turned on, these three valves were actuated at a certain frequency with a certain delay one after another without the control of the computer. Beads added in a buffer solution were pumped by micropump to observe the flow rate. The flow rate is dependent on cycle frequencies, pressure, control channel height and actuation area. The flow rate increased linearly with frequency when frequency was lower than 75Hz[32]. If the frequency was further increased, the flow rate decreased due to incomplete valve opening and closing. There also existed an optimal value for the actuation pressure which turns out to be close to the minimum closure pressure. So a pressure of 20psi was used which was the

minimum pressure for other on-off valves to actuate the micropump. In addition, increase in control channel height or actuation area also leads to a larger flow rate.

Figure 2.6 The image of an integrated peristaltic pump.

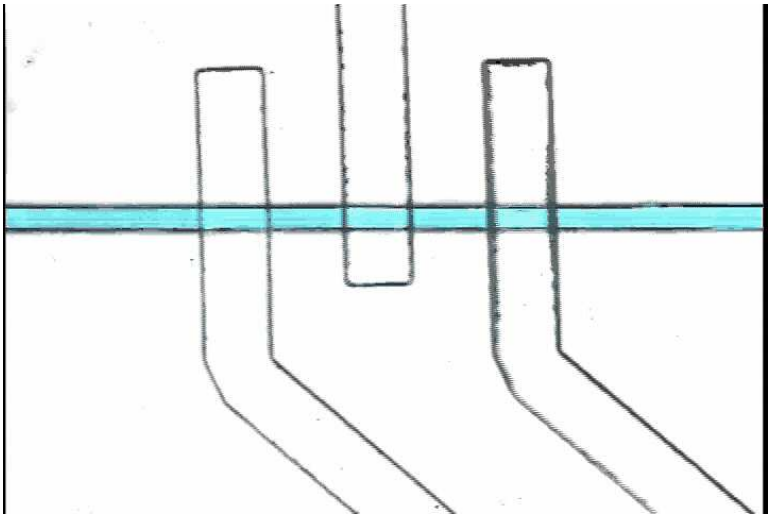

2.4 Transport and isolation of single cells in microfluidic devices

2.4.1. Transport and confine individual cells in the channel

Our aim was to transport cells through microchip channel and confine them individually at the intersection area. We were able to move cells in the channel by integrated peristaltic pump and stop it using the trapping valves. Leukemia Cells were labeled with membrane permeate cytosolic dye Calcein AM and non-permeate Nuclei acid dye Propidium Iodide before loaded onto the chip. Cells labeled with 2μm Calcein AM off chip were loaded into cell reservoir. To trigger the cell flow, the peristaltic pump was actuated at an appropriate cycle frequency. Since it's advantageous to dock the cell to ensure a complete lysate injection before separation, switch valves were used to cut down cell flow and confine the cell at the intersection.

Figure 2.7 Structure of Calcein AM.

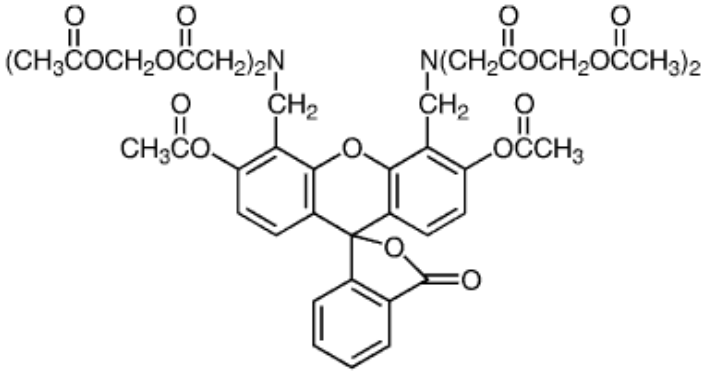

Figure 2.8 Cell labeled with both cytosolic dye--Calcein AM and Nuclei dye--Propidium Iodide

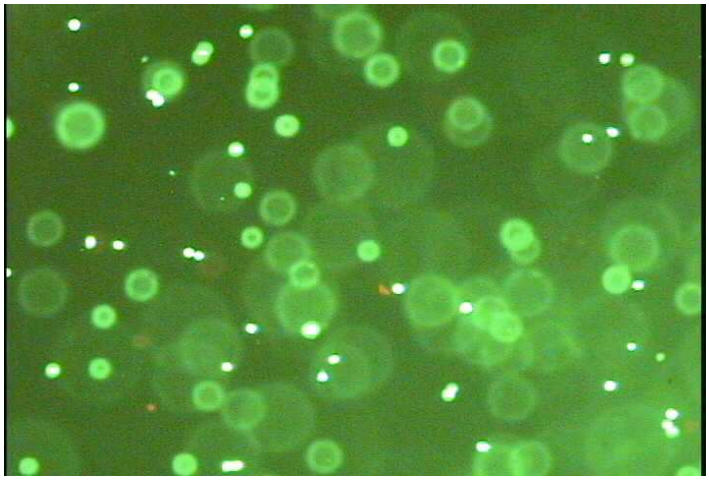

Figure 2.9 Trapping of a single cell at the cross section of a microchip by actuating the valves

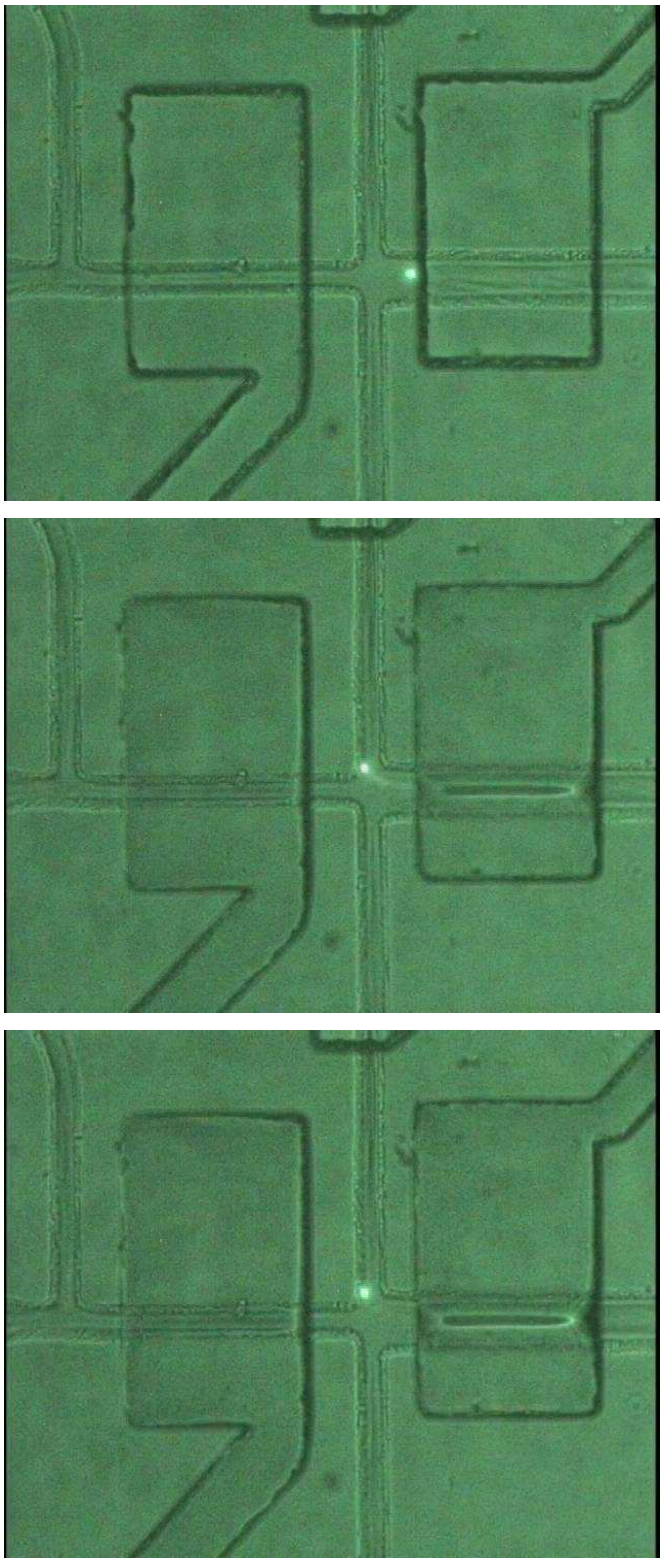

2.4.2. Optimize condition for cell transportation and isolation

Our purpose was to find out an optimal cell flow velocity which can make sure that cells are able to run through the intersection individually and could be stopped by closing the valve ahead of cross-section before lysis.

2.4.2.1 Study the influence of frequency on pumping rate

Cells were pumped through the channel and their velocity was measured to study the influence of the frequency. To observe the cells under fluorescent light, Jurkat cells were labeled with 2μm Calcein AM cytosolic dye. Channels were coated with 2% BSA before running of cells to avoid cell sticking to the side wall of the channel. Our control box can alter the frequency from 5-80Hz with a factor of 2 increments. As Quake has reported, the pumping rate reaches maximum value at 75Hz since the opening and closing of the valves can't be executed completely at high cycle frequencies. In our experiment, the velocity of the cells increases linearly with the increment of the frequency below 80Hz. The maximum pumping rate was obtained at 40Hz with a cell velocity of 1.148mm/s. At frequency of 80Hz, the pumping rate drops to 1.057mm/s. Cell velocity between 1.0-1.5mm/s is appropriate for cell trapping and efficient cell lysis. Also, considering that at frequencies less than 20Hz, the actuation of the pump can be clearly seen and the vibrations of the pumping was so obvious that all the channels could be affected as well as the movement of the cells, we choose 20Hz as our optimal frequency for pumping the cells through the channel.

Figure 2.10 Cell velocity vs. cycle frequency. Cells were pumped at a 100µm by 60µm activation area.

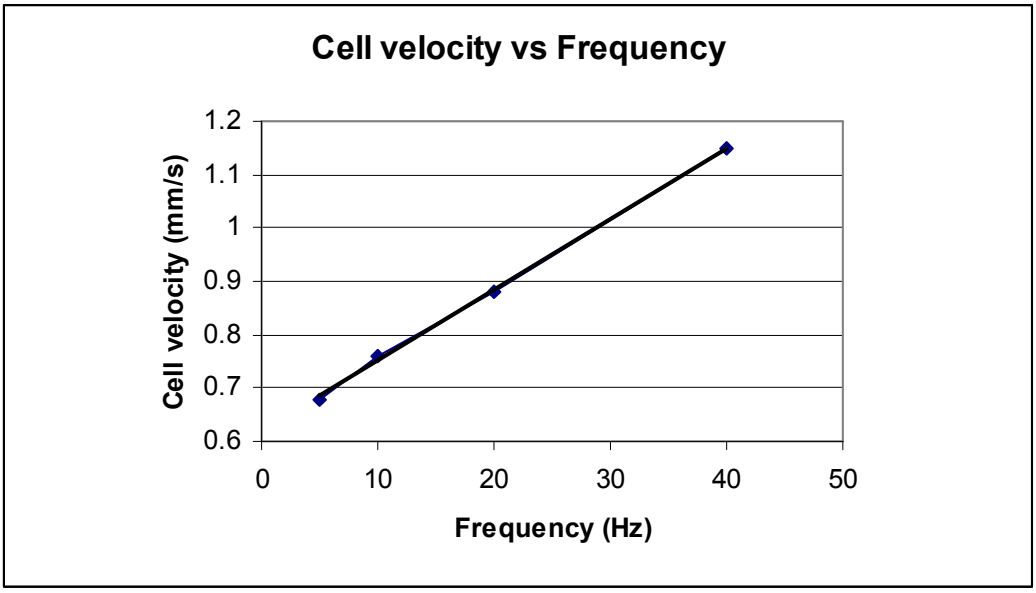

2.4.2.2 Determination of the pump location to optimize pumping performance

The efficiency of the actuation of valves is largely influenced by the active area. The larger the actuation area is, the less pressure is needed to thoroughly close the valve and the faster the fluid can be pumped. We have tried two designs of chips. One has the peristaltic pump located on wide fluid channel with an active area of 100µm by 130µm and the other has the pump on narrow channel with a 100µm by 60µm area. Pumps set on wide channels can generate a maximum cell velocity of 5.737mm/s which is much larger than that can be generated by pumps with the smaller channels. Even at frequency of 10Hz, the cell velocity can reach 3.442mm/s, which is too fast to trap the cell at the intersection. And another problem with pumps on the wide channel is that cells are more likely to be stuck under control channels and some of them are lysed due to slower recovery rate of pumping channels, which leads to easy channel clogging. No such situation happened when pump was located above narrow channel. Based on the advantages of appropriate flow rate for cell trapping and continuous cell flow through the channel, the latter design that the pumps are located on narrow channel was selected for cell transport.

2.4.2.3 Study how valve size affects valve performance

The performance of valve actuation is largely related to the size of valve since the active area determines the amount of pressure needed to actuate the valve. Increasing the width of control channel which consequently enlarges the active area can enhance the performance of valve actuation, which means the fluid channel can be closed more thoroughly at the same pressure with larger valves. In our experiment, for better actuation, the width of our control channels were increased from 55μm to 250μm and the improvement of performance was obvious to see.

As we can see in figure 2.11, even small difference in channel size can lead to big difference in valve performance. When actuated under same pressure simultaneously, valve***1*** which has an active area of is 250μm×55μm only close partially, while valve***2*** with an active area of 250μm×80μm can close completely.

Figure 2.11 The comparison of the effect of valve actuation between 60×250μm and 80 × 250μm active areas.

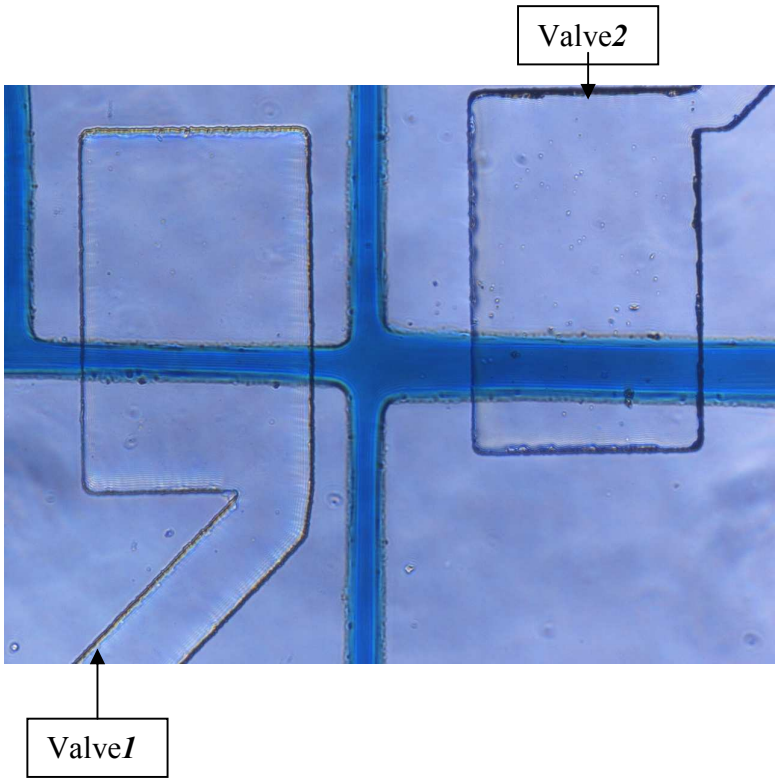

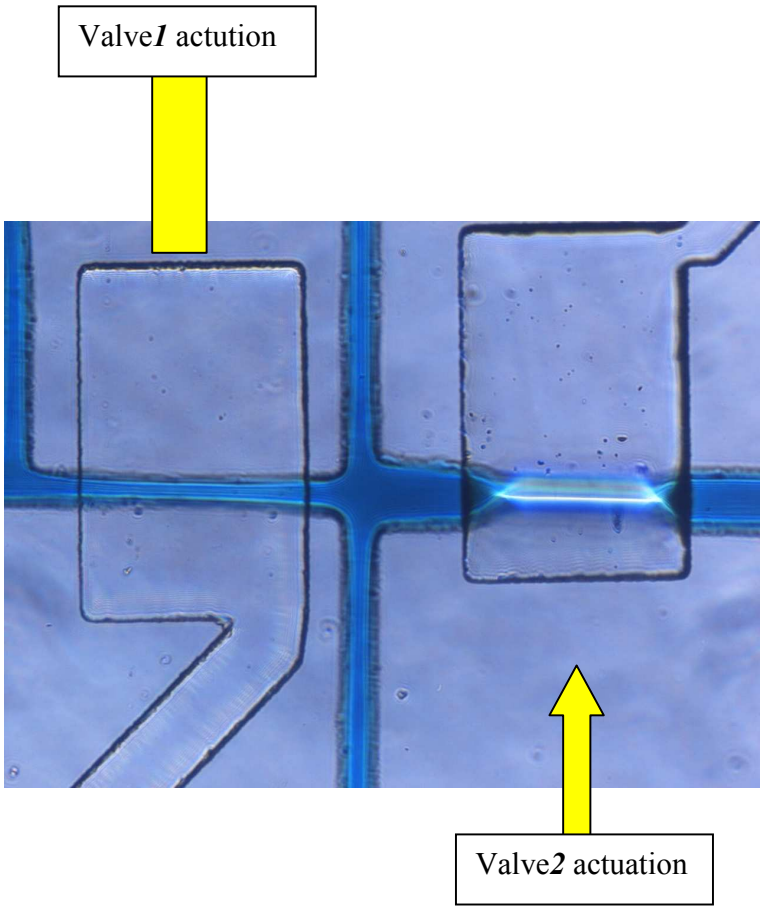

2.4.2.4 Redesign the fluidic channel to reduce pressure driven flow

Except for the flow generated by pumping, there also exists the pressure driven flow that is introduced by gravity due to the various liquid level in reservoirs. Pressure driven flow should be reduced as low as possible since it interferes with the micropump driven flow and causes cells to flow into upper channels instead of moving towards waste reservoirs. Increasing flow resistance of upper channels by lengthening narrow channel is a way to minimize pressure driven flow.

$$U_p = \frac{\Delta p d^2}{l\eta}\left[\frac{1}{12} - \frac{16d}{\pi^5 w}\tanh(\frac{\pi w}{2d})\right] \text{.....(equation 2.1)}^{50}$$

This equation was used to calculate the necessary length of microchip channels to minimize pressure driven flow. Since w›3d in our case, the equation can be simplified as:

$$U_p = \frac{\Delta p d^2}{l\eta} \text{.....(equation 2.2)}$$

According to calculation, the length of narrow channel in upper separation and buffer channels was raised from 2mm to 9mm, so that the pressure driven flow is just one tenth of the pumping rate. By this means, the cells can be transported to the waste reservoir without going up to the upper separation channel.

Chapter 3-Electrical cell lysis and cellular contents separation in microfluidic channels

Electrical lysis was used to break down the cell membrane due to its advantage of fast and selective lysis for those rapid alterable biological reactions which need to be terminated within seconds or even milliseconds. Cell lysis was performed following the detection of individual intact cells and the confinement of the cell at the cross-section. After cell lysis, organelles labeled with specific membrane permeable dyes were separated.

3.1 Using Labview program to control experiments

Multifunction I/O card and Labview VI program were used to accurately control all the processed including monitoring the detection of intact cells by fluorescence, actuating of the control valves to confine the individual cell, triggering applied electric field to lyse the cells and separating and detecting the lysates. When the fluorescence signal from PMT was delivered to the computer through Analog Input (AI) channel, the on-off valves located ahead of intersection were commanded to close the fluid channel. After some delay time for cell to stay at the cross-section, a signal was transported through Analog Output to the power supply, triggering the application of electric field between top and bottom reservoirs to implement cell lysis or subsequent lysate separation. Meanwhile, Data Acquisition started collecting data from PMT and displayed the electropherogram of the separation. After the separation was carried out for 10s, the closed valves were triggered to open again to allow the transportation of cells. Thus, the loop would run again.

Figure 3.1 Flow chart of execution of LabVIEW programs.

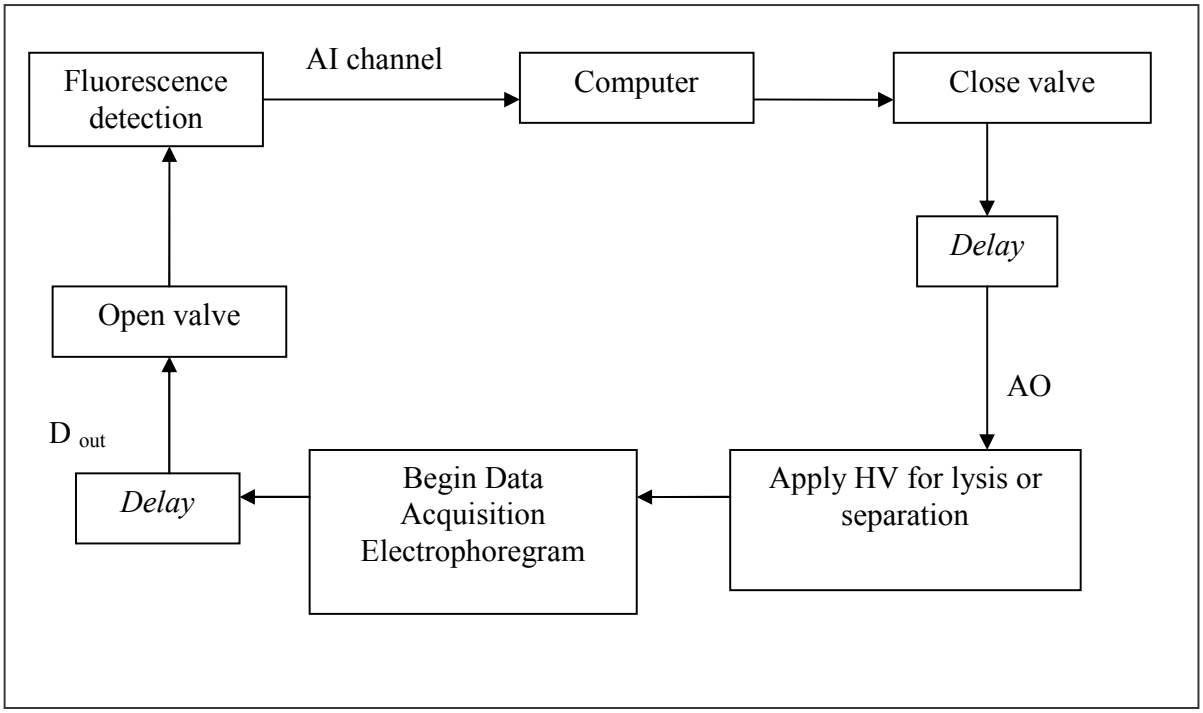

3.2 Detection of intact single cells by fluorescence signals

3.2.1 Cell labeling and loading

In order to detect cells by fluorescence, cells were labeled with fluorescent derivatives before loaded onto the chip. Blood cancer Cells (Leukemia) were used during all the experiments since they grow easily without adhesion to a surface. Cells were labeled with membrane permeate cytosolic dye Calcein AM, Oregon Green 488 and non-permeate Nuclei acid dye Propidium Iodide. Calcein AM and Oregon Green were stored in the DMSO before use. To make a dye solution, stock solution of Calcein AM and Oregon Green was added into PBS with 5mM glucose. The final concentrations for Calcein AM and Oregon Green within the cells were 2μm and 10μm respectively. To label the cells, cells were centrifuged and the suspension media was replaced with the dye solution. After 30 min's incubation, cells were washed with PBS and resuspended in the extracellular buffer which contained 18% Optiprep, 10mM Propidium Iodide, 5mM glucose and 2% BSA in PBS. Propidium Iodide was added into extracellular buffer to indicate cell viability. Cells labeled off chip were loaded into the cell reservoir.

3.2.2 Fluorescence Detection system

The microchip was positioned on the stage of an epi-luminescent microscope. Both 488nm and 514nm laser beam could be obtained from the microscope. The blue light was utilized to detect living single cells while the green light was able to distinguish dead cells which exhibited red color of Propidium Iodide. Cell transportation was monitored through the microscope. The position of the chip was adjusted so that the blue laser spot was exactly placed between the two control valves. The fluorescence signals of an intact cell was collected by a PMT and transferred into the computer to trigger the actuation of those control valves. Signals with high intensity were obtained. The intensity of the signal could be adjusted by tuning the sensitivity knob on the PMT control box. A threshold value of intensity was set to trigger the actuation of two control valves.

Figure 3.2 Schematic of dual detection for both intact cell and cell lysate.

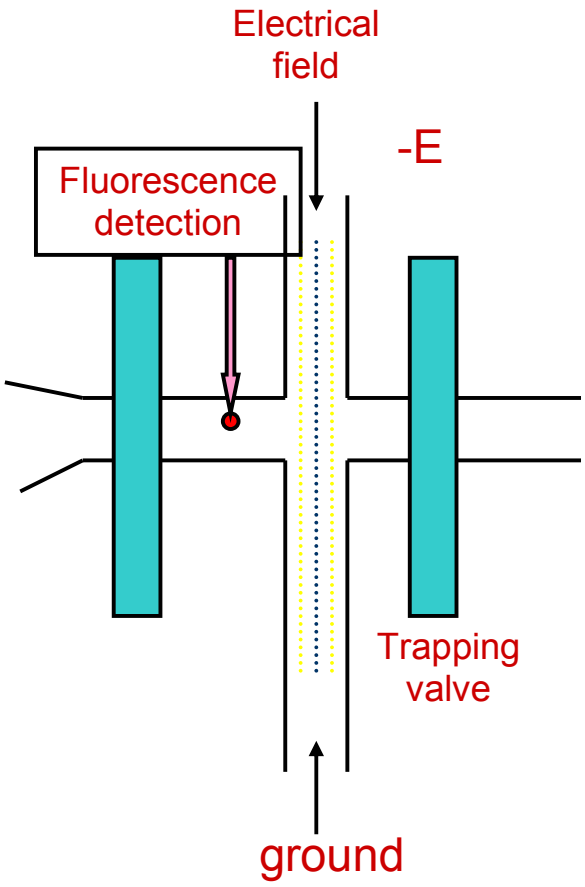

3.3 Implement and optimize electrical cell lysis

Cells were lysed by applying a high electrical field. There are several factors that can affect the efficiency of cell lysis and lysate injection to separation channel. First, cell flow rate was optimized to ensure that single cell can be detected and docked at the intersection. Finally, the flow rate of cell transport was kept at 0.9mm/sec. After the detection of the cell, valves were actuated to terminate the cell flow. Second, the laser spot position where fluorescence detection of intact cells occurred before cell lysis was adjusted to make sure there was sufficient time for cell confinement. Third, the threshold to trigger the actuation of control valve was adjusted so that only signals of intact cells could introduce valve closing. Fourth, temporal actuation of valves to stop the cell and simultaneous lysis pulse relative to the detection of the cell were decided to properly position the cell and completely inject the cell lysate. Fifth, since the efficiency of cell lysis is largely related to the voltage across cell membrane, the amplitude and duration of the applied electrical field were studied to ensure a complete cell lysis as well as lysate injection. We applied an electric field around 850-900 V/cm which was sufficient to lyse the cells completely. The dynamic image of cell lysis was observed through the microscope. The breakdown of the whole cell and cell lysate such as red nuclei acid were observed after the cell lysis. Subsequent images of cell lysis in a video were observed, indicating a rapid cell lysis less than 33ms. Figure 3.3 shows that a single cell is trapped at the cross section by actuating the valves and after applying a high voltage the cell is lysed and intracellular contents are released and separated electrophoretically.

Figure 3.3 Sequential images of cell lysing and lysate injection in the separation channel.

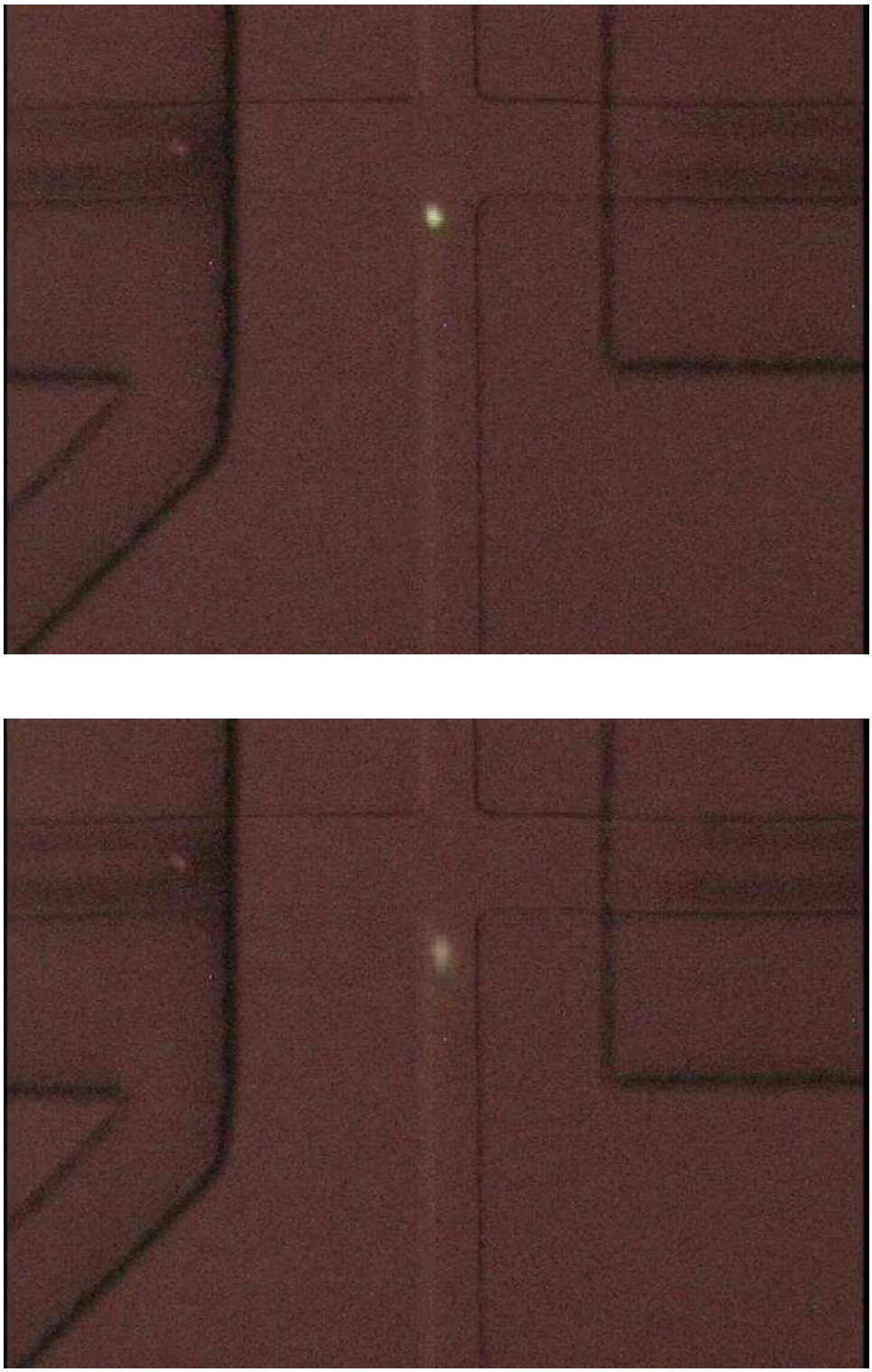

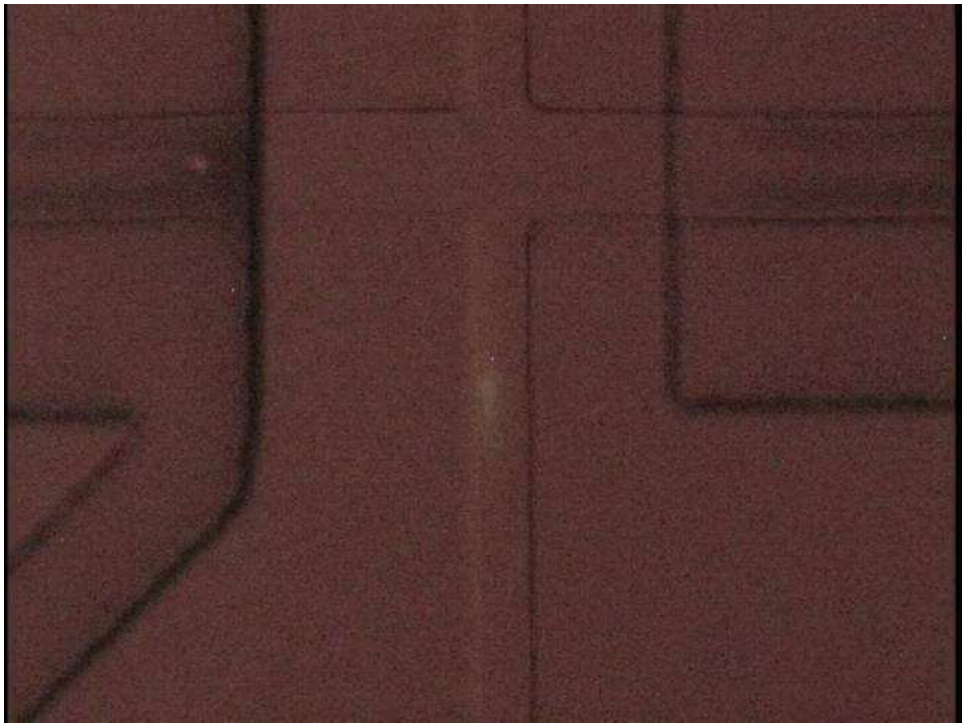

3.4 Separation of fluorescent probes from single cells after cell lysis by electrophoresis

3.4.1. Derivatize cell and cell organelles

To detect various organelles or other cellular contents, cells can be labeled with different fluorescent dyes. Calcein AM were used to label cytosol, DiI was used to track the cell membrane. In addition, Mitotracker Green FM will be used to track mitochondria, Syto 14 will be used to track nucleus, Lysotracker Green DND-26 will be used to track lysosomes, ER-tracker Green dye will be used to track endoplasmic reticulum, Bodipy FL C5-ceramide will be used to track the Gogli apparati and dihydroethidium will be used to track the DNA in the nucleus. Those dyes are all membrane permeable and generally don't show fluorescence until it is introduced into the cell, so background noise will not be an issue. For example, the nonfluorescent Calcein AM becomes a green fluorescent dye after acetoxymethyl ester hydrolysis by intracellular esterases, which turns it into a charged molecule remaining inside the cell. Table shows the excitation and emission wavelength of all of those dyes and this can help decide the wavelength of laser and dichroic mirror used in the single point setup to detect these dyes.

Table 3.1, the excitation and emission wavelength of organelle probes.

Molecular Probes	Binding part	Excitation(nm)	Emission(nm)
Calcein AM	Cytoplasm	490	516
Syto14	Nucleic acids	517	547
DiI	Cell membrane	549	565
Propidium Iodide	Nucleic acids	535	617
Mitotracker Green FM	Mitochondria	490	516
Lysotracker Green DND-	Lysosomes	504	511
ER-tracker Green dye	Endoplasmic reticulum	504	511
Bodipy FL C5-ceramide	Gogli apparati	505	511
Dihydroethidium	DNA	300	610

3.4.2. Detection of analytes by integrated LIF setup

A dual fluorescence detection system was built to detect the intact cells before cell trapping and the cell lysate after cell lysis. A Nikon TS100 inverted microscope was used to provide an X-Y stage for the microchip and an epifluorescence optical setup in the first detection system. Metal light with 488nm wavelength was focused in the transportation channel close to the intersection using a Nikon 20× extra long working distance objective. Emission light was collected through the same objective and traveled through the optical setup within the microscope. The signal was detected using a photomultiplier tube (PMT, MD-952, PerkinElmer, Waltham, MA) after passing through a pinhole and transported to a National Instrument SCB-68-6036E multi-function I/O card (National Instruments) through a control box made by Electronic Devices Lab (EDL) in Kansas State University.

In the second detection system, the excitation light was from an argon ion laser (Melles Griot Laser Group, Carlsbad, CA) which emitted a mixture of 488nm and 514nm light. A 505nm dichroic mirror (505DRLP, Omega Optical, Brattleboro, VT) and a 470nm filter (470AF50, Omega Optical) were used in the optical pathway to remove the green light because only 488nm light was required to excite the dyes. The laser beam was

then focused in the separation channel with a 40× long working distance objective and the emission light was collected through the same objective. The fluorescence emission then passed through a 500nm dichroic mirror (500 DRLP, Omega Optical), spatially filtered by an 800µm pinhole and spectrally filtered with a 525nm (525AF45, Omega Optical). The signal was detected with PMT (MD-952, PerkinElmer) and sampled at 1000 Hz with the same I/O card as used in the first detection system.

Figure 3.4 Schematic of single point setup.

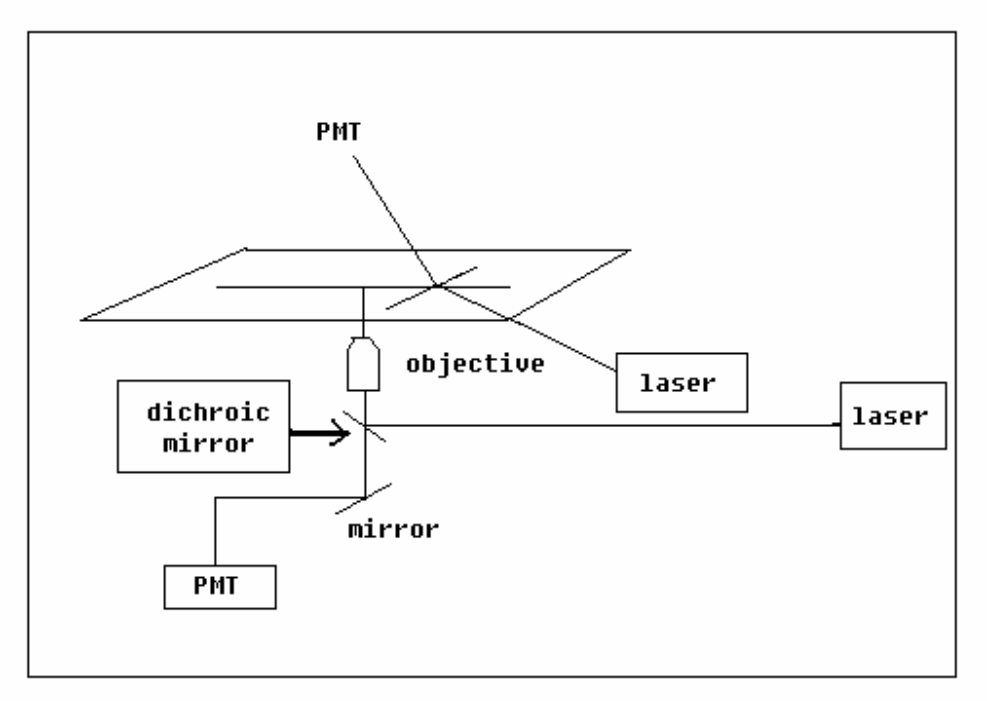

3.4.3 Separation Results

The separation was performed in 10mM NaB, 0.1mM EDTA and 2% BSA and 5% PEG buffer. All of the reservoirs and channels were filled with separation buffer. BSA was added to wet the channels so cells would not adhere to the channel walls and PEG was used to prevent the aggregation of cell lysates. Cells were loaded in the sample reservoir prior to the experiment.

The potential to lyse the cells and separate the lysate electrophoretically was supplied by an in-house power supply. The magnitude of the voltage was controlled by

another 10V power supply. The potential was only applied across the separation channel. The same electric field implemented to lyse the cell was used for the separation.

Various detection distances were examined. A high voltage around 3kV which generated an electric field of 0.85-0.90 kV/cm was applied. The current inside the channel was between 7.5-15 µA resulting in a maximum power dissipation of 1.28 W/m. A single cell was trapped at the cross section by actuating control valves and cell lysates were injected into the separation channel. Detection of a fluorescent dye, Calcein AM or Oregon green diacetate which was loaded into the cell was achieved. The recorded data was analyzed using Igor data analysis software.

Figure 3.5 Electropherogram of a lysed cell loaded with 2µM Calcein AM with a detection distance of 3mm.

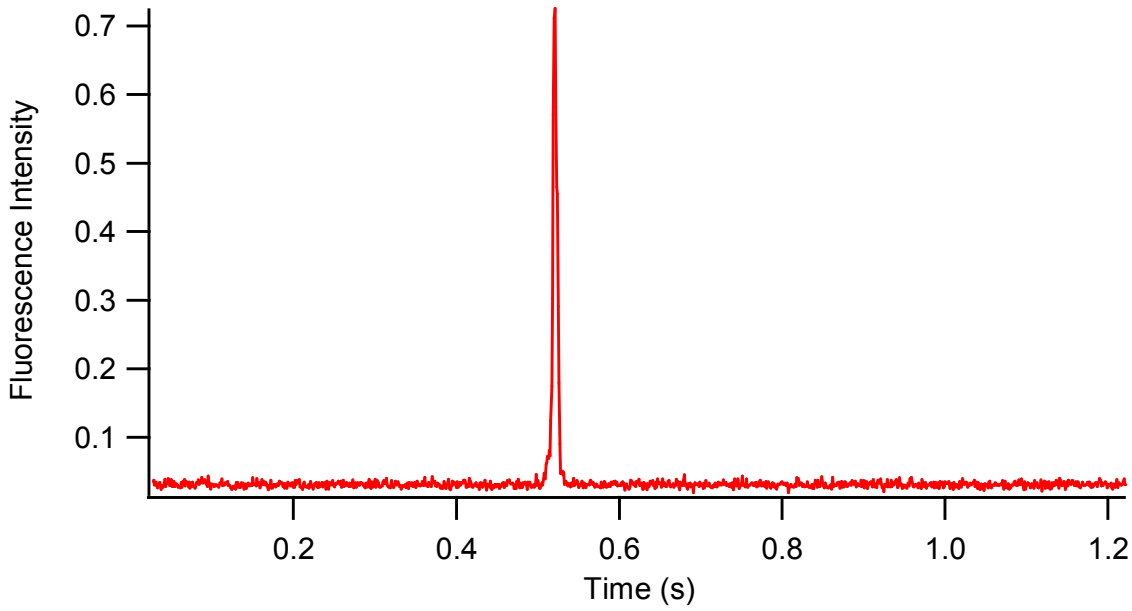

Figure 3.6 Electropherogram of a lysed cell loaded with 2µM Calcein AM with a detection distance of 4mm.

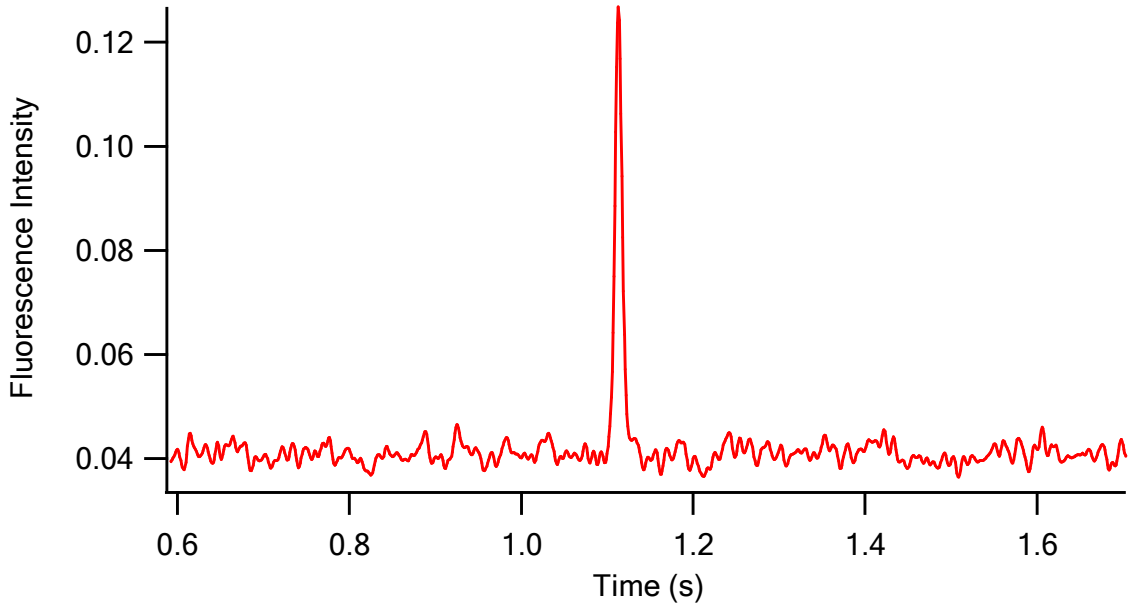

Figure 3.7 Electropherogram of 12 separations of cell lysate containing Calcein AM with a detection distance of 3 mm.

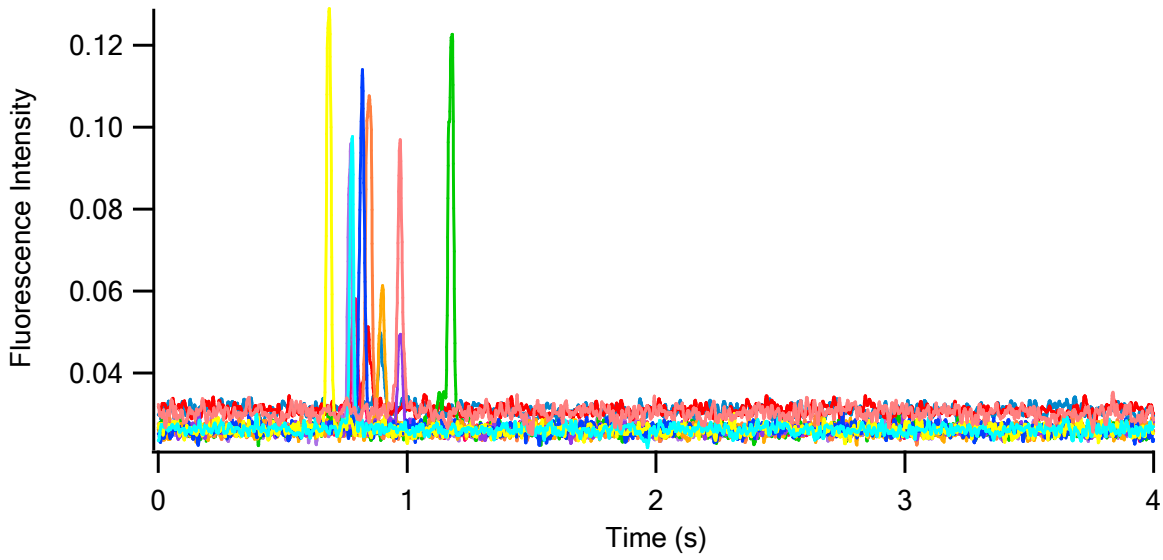

Figure 3.8 Electropherogram of a lysed cell loaded with 2µM Oregon green at detection distance of 3.0mm.

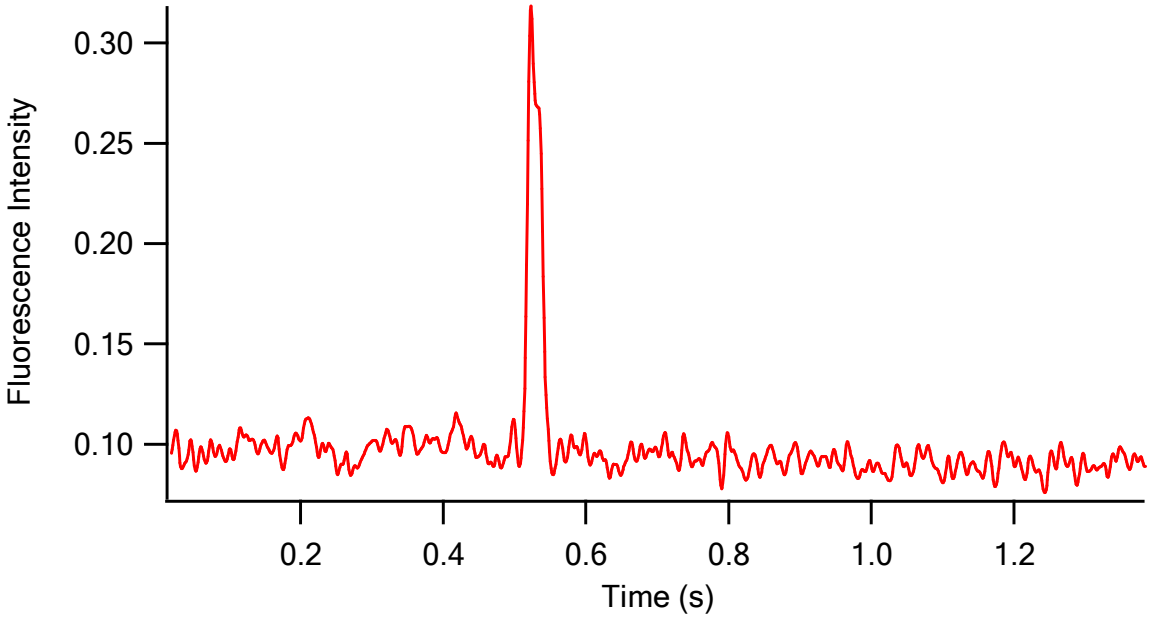

Figure 3.9 Electropherogram of 8 separations of cell lysate from cells loaded with 2µM Oregon green at detection distance of 3.0mm.

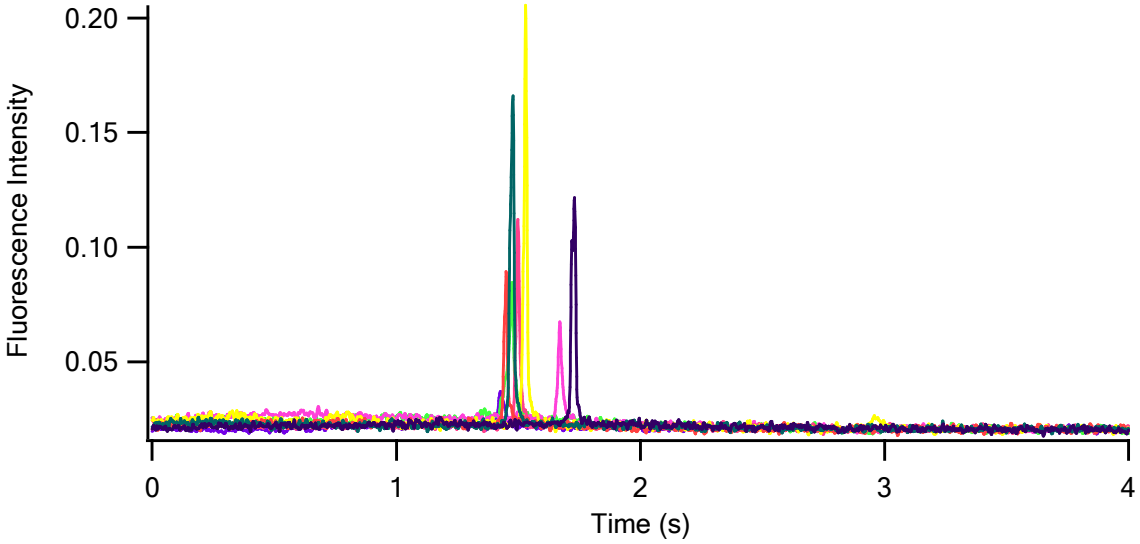

For the separation of both Calcein and Oregon green that were released from single cells, overlapping of those two peaks was observed. With the increase of the migration time, peaks were shown more resolved.

Figure 3.10 Electropherogram of a lysed cell loaded with 2µM Calcein AM and 2µM Oregon green at detection distance of 3mm.

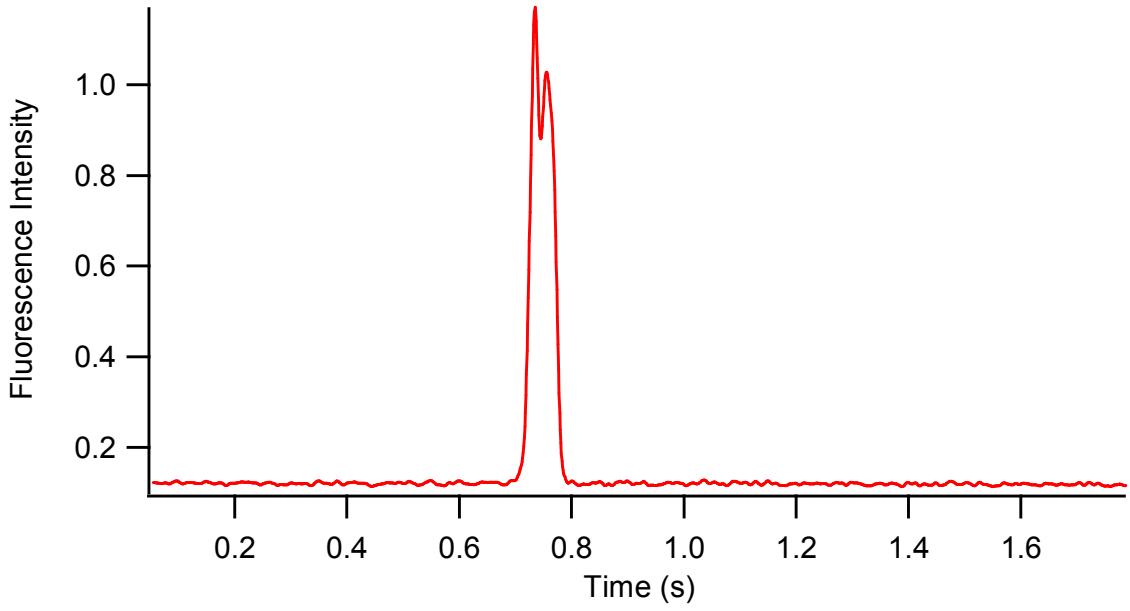

Since single cells were docked at a relatively precise location before lysis and separation, uncertainty of the spatial starting point of cell lysate migration was largely avoided. Figure 3.7 is a combination of 12 peaks that were recorded from the same trials. The average migration time for these fluorescence signals obtained at detection distance of 3mm is 0.87s, with a standard deviation of 0.13 and %RSD of 14.59%. The average width at half maximum of intensity is 0.01s with a standard deviation of 0.002 while the total separation time is 3s. The analyzed data indicate that the band broadening is well controlled. The average number theoretical plates generated is 13133 with a standard deviation of 1758 and %RSD of 13.39 (n=12). For released Calcein AM separations at 4mm, the average migration time increased to 1.00s. The mean of intensity decreases to 0.072, comparing to 0.086 when the separation distance is 3mm. For the Oregon green

separations in figure 3.9, these 8 peaks were obtained from one experiment on the same microchip. The average migration time is 1.53s with a standard deviation of 0.11 and %RSD of 7.08% when detection distance is 3mm. The average width at half maximum intensity is 0.010s with a standard deviation of 0.004 and the mean intensity is 0.11. The average number theoretical plates generated is 7377 with a standard deviation of 492.77 and %RSD of 6.68%. Since the average migration times of Calcein AM and Oregon green are close to one another, the separation of a mixture of these two dyes is not well resolved as shown in figures 3.10. The migration time of cell lysates had a relatively large deviation mainly due to the aggregation of nuclei acids. Irregular flow of fluid in separation channel which contributed to the irreproducible migration time was observed using microscope during the separation. Although several efforts such as adding surfactant such as PEG and using Tris-HCl buffer were made to reduce the aggregation, few positive results were obtained. In order to resolve peaks of Calcein AM and Oregon green, larger separation distances were tried. But due to the clogging problem and the limitation of the sensitivity of fluorescence detection of diluted molecules, signals were hard to be detected. Initial lysis location may have also been a factor since it can affect the absolute migrate time of the lysate.

Chapter-4 Conclusion

We have developed a microfluidic device that can integrate cell transportation, cell lysis and intracellular component separation. This device utilized integrated valves and a pump to transport cells and isolate single cells at the cross section of the channel manifold. Intact cells were first detected and the fluorescent signals triggered the actuation of the control valves. After a single cell was trapped at the intersection, a voltage will be applied to ensure a complete cell lysis and rapid termination of intracellular biochemical reactions. Fluorescent dyes released from single cells were separated electrophoretically and detected using LIF on single point setup. This device can also be used to monitor kinase activities within the cells in the future.

References

(1) Urbanski, J. P.; Thorsen, T.; Levitan, J. A.; Bazant, M. Z. *Applied Physics Letters* **2006**, *89*, 143508/143501-143508/143503.

(2) Roman, G. T.; Chen, Y.; Viberg, P.; Culbertson, A. H.; Culbertson, C. T. *Analytical and Bioanalytical Chemistry* **2007**, *387*, 9-12.

(3) Sims, C. E.; Allbritton, N. L. *Lab on a Chip* **2007**, *7*, 423-440.

(4) Meredith, G. D.; Sims, C. E.; Soughayer, J. S.; Allbritton, N. L. *Nature Biotechnology* **2000**, *18*, 309-312.

(5) Wang, Y.; Hu, S.; Li, H.; Allbritton, N. L.; Sims, C. E. *Journal of Chromatography, A* **2003**, *1004*, 61-70.

(6) Zabzdyr, J. L.; Lillard, S. J. *Analytical Chemistry* **2001**, *73*, 5771-5775.

(7) Shoemaker, G. K.; Lorieau, J.; Lau, L. H.; Gillmor, C. S.; Palcic, M. M. *Analytical Chemistry* **2005**, *77*, 3132-3137.

(8) Han, F.; Wang, Y.; Sims Christopher, E.; Bachman, M.; Chang, R.; Li, G. P.; Allbritton Nancy, L. *Analytical chemistry* **2003**, *75*, 3688-3696.

(9) Li, H.; Sims, C. E.; Kaluzova, M.; Stanbridge, E. J.; Allbritton, N. L. *Biochemistry* **2004**, *43*, 1599-1608.

(10) Soughayer, J. S.; Wang, Y.; Li, H.; Cheung, S.-H.; Rossi, F. M.; Stanbridge, E. J.; Sims, C. E.; Allbritton, N. L. *Biochemistry* **2004**, *43*, 8528-8540.

(11) McClain, M. A.; Culbertson, C. T.; Jacobson, S. C.; Allbritton, N. L.; Sims, C. E.; Ramsey, J. M. *Analytical Chemistry* **2003**, *75*, 5646-5655.

(12) Wang, H.-Y.; Lu, C. *Chemical Communications (Cambridge, United Kingdom)* **2006**, 3528-3530.

(13) Marcus, J. S.; Anderson, W. F.; Quake, S. R. *Analytical Chemistry* **2006**, *78*, 956-958.

(14) Dishinger, J. F.; Kennedy, R. T. *Analytical Chemistry* **2007**, *79*, 947-954.

(15) Gilbert Richard, J.; Park, H.; Rasponi, M.; Redaelli, A.; Gellman, B.; Dasse Kurt, A.; Thorsen, T. *ASAIO J FIELD Full Journal Title:ASAIO journal (American Society for Artificial Internal Organs : 1992)* **2007**, *53*, 447-455.

(16) Duffy Ciaran, F.; Fuller Kathryn, M.; Malvey Megan, W.; O'Kennedy, R.; Arriaga Edgar, A. *Analytical chemistry* **2002**, *74*, 171-176.

(17) Gunasekera, N.; Olson Karen, J.; Musier-Forsyth, K.; Arriaga Edgar, A. *Analytical chemistry* **2004**, *76*, 655-662.

(18) Duffy, C. F.; Gafoor, S.; Richards, D. P.; Admadzadeh, H.; O'Kennedy, R.; Arriaga, E. A. *Analytical Chemistry* **2001**, *73*, 1855-1861.

(19) Anderson Adrian, B.; Xiong, G.; Arriaga Edgar, A. *Journal of the American Chemical Society* **2004**, *126*, 9168-9169.

(20) Luo, C.; Yang, X.; Fu, Q.; Sun, M.; Ouyang, Q.; Chen, Y.; Ji, H. *Electrophoresis* **2006**, *27*, 1977-1983.

(21) Olson, K. J.; Ahmadzadeh, H.; Arriaga, E. A. *Analytical and Bioanalytical Chemistry* **2005**, *382*, 906-917.

(22) Kim, J.; Jang, S. H.; Jia, G.; Zoval, J. V.; Da Silva, N. A.; Madou, M. J. *Lab on a Chip* **2004**, *4*, 516-522.

(23) Di Carlo, D.; Jeong, K.-H.; Lee, L. P. *Lab on a Chip* **2003**, *3*, 287-291.

(24) Schilling, E. A.; Kamholz, A. E.; Yager, P. *Analytical Chemistry* **2002**, *74*, 1798-1804.

(25) Lu, H.; Schmidt, M. A.; Jensen, K. F. *Lab on a Chip* **2005**, *5*, 23-29.
(26) Wang, H.-Y.; Bhunia, A. K.; Lu, C. *Biosensors & Bioelectronics* **2006**, *22*, 582-588.
(27) Tsong, T. Y. *Biophysical Journal* **1991**, *60*, 297-306.
(28) Ramadan, Q.; Samper, V.; Poenar, D.; Liang, Z.; Yu, C.; Lim, T. M. *Sensors and Actuators, B: Chemical* **2006**, *B113*, 944-955.
(29) Wang, H.-Y.; Lu, C. *Analytical Chemistry* **2006**, *78*, 5158-5164.
(30) Wang, H.-Y.; Lu, C. *Biotechnology and Bioengineering* **2006**, *95*, 1116-1125.
(31) Khine, M.; Ionescu-Zanetti, C.; Blatz, A.; Wang, L.-P.; Lee, L. P. *Lab on a Chip* **2007**, *7*, 457-462.
(32) Unger, M. A.; Chou, H.-P.; Thorsen, T.; Scherer, A.; Quake, S. R. *Science (Washington, D. C.)* **2000**, *288*, 113-116.
(33) Lu, C.; Lee, I. C.; Masel, R. I.; Wieckowski, A.; Rice, C. *Journal of Physical Chemistry A* **2002**, *106*, 3084-3091.
(34) Fu, A. Y.; Chou, H.-P.; Spence, C.; Arnold, F. H.; Quake, S. R. *Analytical Chemistry* **2002**, *74*, 2451-2457.
(35) Oblak, T. D. A.; Root, P.; Spence, D. M. *Analytical Chemistry* **2006**, *78*, 3193-3197.
(36) Thompson, H. G. R.; Harris, J. W.; Wold, B. J.; Quake, S. R.; Brody, J. P. *Genome Research* **2002**, *12*, 1517-1522.
(37) Goulpeau, J.; Trouchet, D.; Ajdari, A.; Tabeling, P. *Journal of Applied Physics* **2005**, *98*, 044914/044911-044914/044919.
(38) Li Michelle, W.; Huynh Bryan, H.; Hulvey Matthew, K.; Lunte Susan, M.; Martin, R. S. *Analytical chemistry* **2006**, *78*, 1042-1051.
(39) Hong Jong, W.; Studer, V.; Hang, G.; Anderson, W. F.; Quake Stephen, R. *Nature biotechnology* **2004**, *22*, 435-439.
(40) Thorsen, T.; Maerkl, S. J.; Quake, S. R. *Science (Washington, DC, United States)* **2002**, *298*, 580-584.
(41) Marcus Joshua, S.; Anderson, W. F.; Quake Stephen, R. *Analytical chemistry* **2006**, *78*, 956-958.
(42) Wheeler, A. R.; Throndset, W. R.; Whelan, R. J.; Leach, A. M.; Zare, R. N.; Liao, Y. H.; Farrell, K.; Manger, I. D.; Daridon, A. *Analytical Chemistry* **2003**, *75*, 3581-3586.
(43) Meyer, A. R.; Clark, A. M.; Culbertson, C. T. *Abstracts, 40th Midwest Regional Meeting of the American Chemical Society, Joplin, MO, United States, October 26-29* **2005**, LIN05-130.
(44) Di Carlo, D.; Lee, L. P. *Analytical Chemistry* **2006**, *78*, 7918-7925.
(45) Yamamura, S.; Kishi, H.; Tokimitsu, Y.; Kondo, S.; Honda, R.; Rao, S. R.; Omori, M.; Tamiya, E.; Muraguchi, A. *Analytical Chemistry* **2005**, *77*, 8050-8056.
(46) Wang, Z.; Kim, M.-C.; Marquez, M.; Thorsen, T. *Lab on a Chip* **2007**, *7*, 740-745.
(47) Tamaki, E.; Sato, K.; Tokeshi, M.; Sato, K.; Aihara, M.; Kitamori, T. *Analytical Chemistry* **2002**, *74*, 1560-1564.
(48) Cellar Nicholas, A.; Burns Scott, T.; Meiners, J.-C.; Chen, H.; Kennedy Robert, T. *Analytical chemistry* **2005**, *77*, 7067-7073.

(49) Uchiyama, K.; Nakajima, H.; Hobo, T. *Analytical and Bioanalytical Chemistry* **2004**, *379*, 375-382.
(50) Jacobson, S. C.; Culbertson, C. T. *Separation Methods in Microanalytical Systems* **2006**, 19-54.
(51) Culbertson, C. T.; Jacobson, S. C.; Ramsey, J. M. *Analytical Chemistry* **2000**, *72*, 5814-5819.
(52) Roper Michael, G.; Shackman Jonathan, G.; Dahlgren Gabriella, M.; Kennedy Robert, T. *Analytical chemistry* **2003**, *75*, 4711-4717.
(53) El-Ali, J.; Sorger, P. K.; Jensen, K. F. *Nature (London, United Kingdom)* **2006**, *442*, 403-411.
(54) Nishiyama, T.; Endo, F.; Eguchi, H.; Tsunokawa, J.; Nakagama, T.; Seino, N.; Shinoda, M.; Shimosaka, T.; Hobo, T.; Uchiyama, K. *Chemistry Letters* **2006**, *35*, 272-273.
(55) Di Carlo, D.; Ionescu-Zanetti, C.; Hung, P. J.; Zhang, Y.; Lee, L. P. *Special Publication - Royal Society of Chemistry* **2004**, *297*, 165-167.
(56) Ionescu-Zanetti, C.; Wang, L.-P.; Di Carlo, D.; Hung, P.; Di Blas, A.; Hughey, R.; Lee Luke, P. *Cytometry A FIELD Full Journal Title:Cytometry. Part A : the journal of the International Society for Analytical Cytology* **2005**, *65*, 116-123.
(57) Lee, C.-Y.; Lee, G.-B.; Lin, J.-L.; Huang, F.-C.; Liao, C.-S. *Journal of Micromechanics and Microengineering* **2005**, *15*, 1215-1223.
(58) El-Ali, J.; Gaudet, S.; Guenther, A.; Sorger, P. K.; Jensen, K. F. *Analytical Chemistry* **2005**, *77*, 3629-3636.
(59) Poulsen, C. R.; Ramsey, J. M. *Special Publication - Royal Society of Chemistry* **2004**, *297*, 162-164.
(60) Lapizco-Encinas, B. H.; Simmons, B. A.; Cummings, E. B.; Fintschenko, Y. *Analytical Chemistry* **2004**, *76*, 1571-1579.
(61) Shackman, J. G.; Dahlgren, G. M.; Peters, J. L.; Kennedy, R. T. *Lab on a Chip* **2005**, *5*, 56-63.
(62) Wang, Y.; Lai, H.-H.; Bachman, M.; Sims, C. E.; Li, G. P.; Allbritton, N. L. *Analytical Chemistry* **2005**, *77*, 7539-7546.
(63) Murthy, S. K.; Sethu, P.; Vunjak-Novakovic, G.; Toner, M.; Radisic, M. *Biomedical Microdevices* **2006**, *8*, 231-237.
(64) Coe, B. J.; Thompson, D. W.; Culbertson, C. T.; Schoonover, J. R.; Meyer, T. J. *Inorganic Chemistry* **1995**, *34*, 3385-3395.
(65) Medley Colin, D.; Drake Timothy, J.; Tomasini Jeffrey, M.; Rogers Richard, J.; Tan, W. *Analytical chemistry* **2005**, *77*, 4713-4718.
(66) Marcus, J. S.; Anderson, W. F.; Quake, S. R. *Analytical Chemistry* **2006**, *78*, 3084-3089.
(67) Abruzzo, L. V.; Lee, K. Y.; Fuller, A.; Silverman, A.; Keating, M. J.; Medeiros, L. J.; Coombes, K. R. *BioTechniques* **2005**, *38*, 785-792.
(68) Messina, G. A.; De Vito, I. E.; Raba, J. *Analytica Chimica Acta* **2006**, *559*, 152-158.
(69) Tanaka, Y.; Sato, K.; Yamato, M.; Okano, T.; Kitamori, T. *Analytical Sciences* **2004**, *20*, 411-413.

(70) Ocvirk, G.; Salimi-Moosavi, H.; Szarka, R. J.; Arriaga, E. A.; Andersson, P. E.; Smith, R.; Dovichi, N. J.; Harrison, D. J. *Proceedings of the IEEE* **2004**, *92*, 115-125.
(71) Di Carlo, D.; Wu, L. Y.; Lee, L. P. *Lab on a Chip* **2006**, *6*, 1445-1449.